Novel Fouling-Reducing Coatings for Ultrafiltration, Nanofiltration, and Reverse Osmosis Membranes

Final Scientific/Technical Report

Reporting Period Start Date: 1 September 2004

Reporting Period End Date: 31 August 2008

Principal Author: Dr. Benny D. Freeman

Date of Report: 29 November 2008

DOE Award Number: DE-FC26-04NT15547

Submitting Organization: The University of Texas at Austin

Center for Energy & Environmental Resources

and Department of Chemical Engineering

10100 Burnet Road, Building 133

Austin, TX 78758

ABSTRACT

Polymeric membranes could potentially be the most flexible and viable long-term strategy for treatment of produced water from oil and gas production. However, widespread use of membranes, including reverse osmosis (RO) membranes, for produced water purification is hindered due to fouling caused by the impurities present in the water. Fouling of RO membranes is likely caused by surface properties including roughness, hydrophilicity, and charge, so surface modification is the most widely considered approach to improve the fouling properties of current RO membranes. This project focuses on two main approaches to surface modification: coating and grafting. Hydrophilic coating and grafting materials based on poly(ethylene glycol) (PEG) are applied to commercial RO membranes manufactured by Dow FilmTec and GE. Crossflow filtration experiments are used to determine the fouling resistance of modified membranes, and compare their performance to that of unmodified commercial RO membranes. Grafting and coating are shown to be two alternative methods of producing modified membranes with improved fouling resistance.

TABLE OF CONTENTS

EXECUTIVE SUMMARY

Polymeric membranes could potentially be the most flexible and viable long-term strategy for treatment of produced water from oil and gas production, including removal of salts, emulsified oil, other organics and particulates. Depending on the impurities present and the level of purification required, reverse osmosis (RO), nanofiltration (NF), or ultrafiltration (UF) membranes can be used. An inherent drawback of all membranes, including RO, NF, and UF, is that they experience fouling by impurities present in the water. The problem is exacerbated when these membranes are exposed to a mixture of impurities such as salt, emulsified oil droplets, and other particulate matter, and their lifetime decreases dramatically due to largely irreversible membrane fouling.

Two types of fouling may occur, surface and internal. Surface fouling occurs when particles deposited on the membrane surface precipitate, reducing flow through the membrane. This type of fouling is also strongly dependent on interactions between contaminants and the membrane surface. RO and NF membranes have very rough surfaces and a high chemical affinity for oil and other organic components of produced water, characteristics causing their extreme susceptibility to surface fouling by organics. Internal fouling is caused by penetration of particulates into the membrane interior, where they block pores and reduce water flux. Internal fouling is essentially irreversible because the particles accumulate inside the pores and are then resistant to even aggressive chemical and hydrodynamic cleaning procedures. UF membranes are porous and therefore subject to internal fouling by particulates, organics, and other components of wastewater. Thus, fouling is a barrier to more widespread application of membranes for produced water purification.

One approach to improve fouling resistance of commercial RO, NF, and UF membranes is to apply a very thin (on the order of 0.5 microns), nonporous, hydrophilic coating to the surface. The coating should be very water-permeable and simultaneously resist both internal and surface fouling. Due to the nonporous nature of the coating, particles are not able to reach the underlying membrane structure, reducing pore blockage and internal fouling. Additionally, surface fouling is diminished because the coating itself resists adhesion of emulsified oil droplets. Another approach to reduce membrane fouling is to graft molecules to the membrane surface to alter the surface characteristics. These molecules may either be hydrophilic for a direct enhancement of surface hydrophilicity, or may provide double bonds on the membrane surface which permit surface polymerization with a hydrophilic monomer.

This project focused on surface modification of commercial RO membranes by coating and grafting hydrophilic materials to the membrane surface. First, the commercial RO membranes, the LE and XLE by Dow FilmTec and the AG from GE, were thoroughly characterized. Crossflow testing conditions must be

carefully controlled in order to measure accurate, reliable values of water flux and NaCl rejection in accordance with the manufacturer's specifications. Feed pH and the use of prefiltration of the feed water were found to be critical variables in membrane testing. The LE/XLE and AG membranes must be tested under different conditions (pH 8 with unprefiltered feed and pH 7 with prefiltered feed, respectively) to obtain their best performance. Concentration polarization also must be accounted for to find the true salt rejection capabilities of the membranes.

Before applying coatings to membranes, thorough characterization of the coating materials was performed. Three series of PEG-based copolymers were systematically studied to relate chemical composition and structure to polymer properties such as water and NaCl permeability. Acrylic acid, 2-hydroxyethyl acrylate, or poly(ethylene glycol) acrylate were each copolymerized with poly(ethylene glycol) diacrylate to form a highly hydrophilic, crosslinked hydrogel. All of the copolymers exhibited large water uptake, with the PEGA copolymers having the largest uptake amounts. Water permeability was directly proportional to the water uptake; higher water uptake materials also had higher water permeability, regardless of chemical composition. Ethylene oxide content and crosslink density were major contributors to water sorption and transport behavior. Increasing ethylene oxide content and decreasing crosslink density both promoted increased water transport. NaCl diffusion and partition coefficients were also measured. The salt transport properties were similar to the water transport properties; higher water uptake materials also had a larger salt uptake, and high water permeability lead to large diffusion coefficients and high salt permeability. Contact angle measurements confirmed the hydrophilic nature of the copolymer surfaces. All copolymer contact angles were less than the contact angle of a commercial RO membrane, indicating that the copolymer surfaces would be less conducive to oil adhesion.

RO membranes were successfully coated with a dense layer of the abovementioned hydrogels. Based on water flux measurements of coated membranes, coatings were on the order of 1 to 2 microns. Salt rejection measurements showed that coatings do no negatively impact salt rejection. In fact, often salt rejection of a coated membrane is slightly higher than that of an uncoated membrane. Coated membranes were subjected to various foulants and fouling solutions. All of the coatings showed excellent fouling resistance in the presence of cationic surfactants.

Grafting of hydrophilic PEG molecules was performed by reaction of membrane surface amine groups with the epoxide endgroups of poly(ethylene glycol) diglycidyl ether (PEG diepoxide). XLE RO membranes and NF90 nanofiltration membranes (with the same polyamide surface chemistry as the XLE RO membranes) were dip coated or top surface-treated in heated solutions of PEG diepoxide for 10 minutes to ensure reaction with the membrane surface. Dead end and crossflow water flux and NaCl rejection testing revealed the effect of

PEG diepoxide molecular weight and concentration on surface coverage, water flux, and NaCl rejection. Crossflow testing of high water flux candidates demonstrated that PEG diepoxide-grafted NF90 and XLE membranes have better fouling resistance than their unmodified counterparts (LE and XLE membranes).

EXPERIMENTAL METHODS

Task 1: Emulsion Selection, Preparation, and Characterization

Two produced water emulsion samples were obtained and analyzed in concert with the U.S. Bureau of Reclamation, also interested produced water membrane fouling studies. Two produced water samples from the southwest region of the United States were obtained, one from a natural gas well and one from an oil well. The samples were analyzed by Crystal Solutions (Laramie, WY) using EPA and AWWA standards.

Model emulsions for fouling studies consisted of 9 parts oil (*n*-decane, or *n*-dodecane) to one part surfactant. Dodecyltrimethylammonium bromide (DTAB), and sodium dodecyl sulfate (SDS) were chosen as representative, cationic, and anionic surfactants, respectively (cf., Figure 1). Emulsion preparation consisted of mixing the oil, surfactant, and deionized water (Millipore MilliQ, 18 MΩ, 1.2 ppb) in a Waring blender on high speed for 3 minutes.

Dodecyltrimethylammonium bromide (DTAB)

Sodium dodecyl sulfate (SLS)
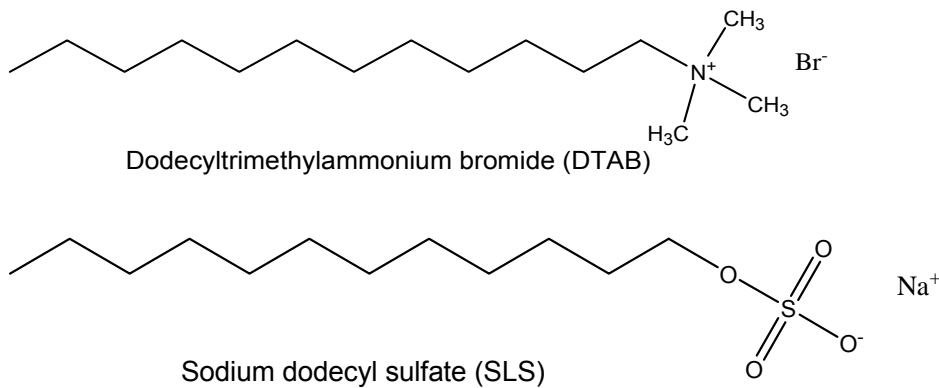
Figure 1. Chemical structures of surfactants.

Emulsion droplet size distribution and stability were estimated using a Carl Zeiss AxioSkop Optical Microscope. Droplet sizes were measured using AxioVision LE software. Latex particles of known diameter were used to calibrate the microscope. Droplet number average diameter, d_N, was calculated using the equation:

$$d_N = \frac{\sum N_i d_i}{\sum N_i} \tag{1}$$

Droplet volume average diameter, d_v, was calculated using the equation:

$$d_v = \frac{\sum N_i d_i^4}{\sum N_i d_i^3} \tag{2}$$

The polydispersity index, PDI, an indication of droplet size distribution, was calculated from d_N and d_v:

$$PDI = \frac{d_v}{d_N} \qquad\qquad (3)$$

Task 2: Selection of Commercial Membrane Supports

Flat-sheet AG RO membranes manufactured by GE Infrastructure Water Process and Technologies were used for characterization and modification studies. The AG membrane is a commercial brackish water desalination RO membrane (50 L/(m^{2}h) (LMH) water flux at 225 psig, 98-99% NaCl rejection)[1] and is a polyamide thin film composite membrane representative of the vast majority of commercial RO and NF membranes available today. The generic structure of the polyamide layer, which provides salt rejection in this membrane, is:
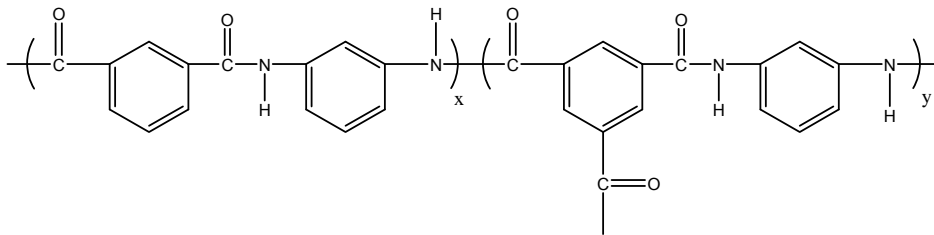

Flat-sheet membranes from DOW Water Solutions were also obtained for use in characterization and modification studies. They include the LE (low energy, 49 LMH flux at 150 psi, 99.0-99.3% NaCl rejection)[2] and XLE (extra low energy, 67 LMH at 150 psi, 98.0-99.0% NaCl rejection)[3] reverse osmosis membranes. In addition, a higher flux nanofiltration membrane, the NF90, was included for modification studies. The NF90 membrane achieves a water flux of 109 LMH in a 2000 ppm NaCl feed at 150 psi, with a NaCl rejection in the range 85-95%. These membranes all share the same general chemical structure shown above. The XLE and NF90 membranes will be used for modification studies, while the LE will be used as a control for comparison with the modified membranes. Surface modification decreases water flux, so comparing a control membrane with a pure water flux similar to that of the modified membrane will provide a better gauge of the fouling resistance of the modified membranes.

Task 3: Synthesis and Characterization of Fouling-Resistant Materials

UV-polymerized hydrogels were synthesized as potential fouling-resistant coatings. The crosslinking agent, poly(ethylene glycol) diacrylate (PEGDA), was obtained from Sigma-Aldrich (Milwaukee, WI) and used as received. The monomers, poly(ethylene glycol) acrylate (PEGA), 2-hydroxyethyl acrylate (HEA), and acrylic acid (AA) (cf., Figure 2), were obtained from Sigma-Aldrich and used without further purification. These three monomers were chosen to

systematically study the effects of comonomer chain length, i.e., the number of ethylene oxide (EO) units, on material properties. Each monomer has an acrylic endgroup and a hydroxyl endgroup. However, AA does not contain any EO units, HEA contains one unit, and PEGA contains seven units. The photoinitiator was 1-hydroxycyclohexyl phenyl ketone (HPK), also obtained from Sigma-Aldrich.

Poly(ethylene glycol) diacrylate (PEGDA)

Poly(ethylene glycol) acrylate (PEGA)

2-Hydroxyethyl acrylate (HEA)

Acrylic Acid (AA)
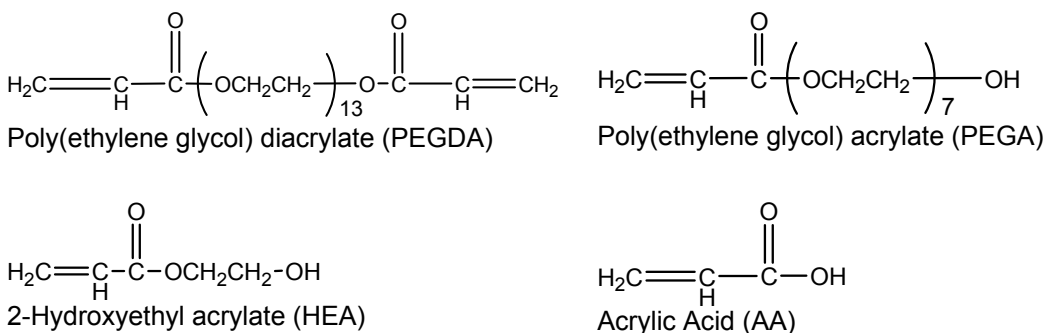
Figure 2. Chemical structures of materials used.

Prepolymerization mixtures were prepared by combining desired amounts of crosslinker and monomer with a specified amount of deionized (DI) water and 1.0 wt% (based on solids content) of photoinitiator. The crosslinker, monomer, and photoinitiator were first mixed in an amber glass jar and stirred with a magnetic stir bar for approximately one hour until the photoinitiator dissolved. An amber glass jar was used to minimize the solution exposure to light. After the photoinitiator dissolved, the appropriate amount of DI water was added, and the solution was stirred for an additional hour before use. For the materials prepared in this study, the water content in the prepolymerization mixture was 60 wt%, based on total mixture weight. The films were named based on monomer content and monomer type. For example, a 60PEGA film was polymerized from an initial mixture containing 60 mole% PEGA and 40 mole% PEGDA, with 60 wt% water in the prepolymerization mixture.

Free-standing dense films were prepared by first placing the prepolymerization mixture between two quartz plates, using spacers to control film thickness. Then, the mixture was exposed to 312 nm wavelength UV-light for 90 s at 3000 $\mu W/cm^2$ in a Fisher-Scientific UV-Crosslinking chamber (Pittsburgh, PA). Films were removed from the quartz plates, rinsed, and soaked in DI water until used. Sol fractions in the hydrogels were found to be negligible after a 5 day extraction in water. This behavior is supported by previous work on similar copolymer materials[4]. Therefore, no further extraction was performed apart from rinsing and storing in DI water.

Hydrogel water sorption was measured. Free-standing hydrogel films were equilibrated in DI water for a minimum of one hour. The films were then patted dry with ChemWipe tissues and weighed using an analytical balance. After

weighing, the samples were dried under vacuum overnight and then weighed again. The water volume fraction, v_s, is calculated by assuming additive mixing:

$$v_{H_2O} = \frac{\dfrac{m_{wet} - m_{dry}}{\rho_{H_2O}}}{\dfrac{m_{wet} - m_{dry}}{\rho_{H_2O}} + \dfrac{m_{dry}}{\rho_{polymer}}} \tag{4}$$

where m_{wet} is the mass of the wet film, m_{dry} is the mass of the dry film, ρ_{H2O} is the density of water, and $\rho_{polymer}$ is the polymer film density.

Hydrogel water flux was measured using dead-end filtration operated at different transmembrane pressures. Advantec MFS, Inc. UHP 43 (diameter 43mm) dead-end stirred filtration cells (Dublin, CA) were used at pressures ranging from 1.7 to 4.5 bar (10-50 psig) at 25°C. Permeate volume, V, as a function of time, t, was recorded, and water flux, J_{H_2O}, was calculated as follows:

$$J_{H_2O} = \frac{\Delta V}{\Delta t} \frac{1}{A} \tag{5}$$

where A is active hydrogel area. Then, water flux was used to calculate water permeability, P_{H_2O}:

$$P_{H_2O} = \frac{J_{H_2O} \ell}{\Delta p} \tag{6}$$

where ℓ is film thickness, and Δp is the applied transmembrane pressure difference. Ultrapure water from a Millipore MilliQ system (18.2 MΩ, 1.2 ppb) was used in all experiments. Film thickness was measured using a Mitutoyo Absolute micrometer (Model ID-C112E, Mitutoyo USA, Aurora, IL) following guidelines in ISO 9339-2[5]. Water flux was measured at a minimum of three pressures, and average water permeability was calculated by averaging the individual permeabilities.

Salt transport in hydrogel films was evaluated using kinetic salt desorption experiments[6,7]. A hydrogel film was immersed in 50 cm^3 of 5 wt% NaCl dissolved in DI water (i.e., the so-called "donor" solution). After 24 hours, the film was removed from the donor solution and quickly patted dry. The film was then placed in a beaker containing 50 cm^3 of DI water, and the beaker was sealed with Parafilm to minimize CO_2 absorption and changes in solution conductivity that accompany CO_2 absorption. The solution was stirred at approximately 300 rpm to ensure a constant salt concentration throughout the liquid in the beaker. The conductivity of the solution was measured as a function of time at 25°C using an InoLab WTW 730 Conductivity meter (WTW, Woburn, MA), and the data were recorded at 5 second intervals. Conductivity was converted to NaCl concentration using a calibration curve.

The diffusion coefficient of NaCl in the hydrogel film was calculated based on a Fickian analysis of desorption from a planar film[8,9]. M_t/M_∞ was plotted versus

$t^{1/2}$, where M_t is the mass of salt in the initially pure water solution at time t, and M_∞ is the total amount of salt desorbed from the polymer into the solution. For $0.1 < M_t/M_\infty < 0.6$, M_t/M_∞ is expected to be a linear function of $t^{1/2}$ [6]. The diffusion coefficient, D_s, was calculated as follows[8,9]:

$$\frac{d(M_t/M_\infty)}{d(t^{1/2})} = \frac{4}{\ell}\left(\frac{D_s}{\pi}\right)^{1/2} \quad (7)$$

where $d(M_t/M_\infty) / d(t^{1/2})$ is the slope in the linear region of a plot of M_t/M_∞ versus $t^{1/2}$, and ℓ is the thickness of the hydrated film used in the salt desorption experiments.

The salt partition coefficient, K_s, is the ratio of the mass of NaCl in the polymer, M_∞, per unit hydrogel volume to the mass of NaCl in the original solution per volume of original solution (i.e., $\dfrac{\text{g NaCl}/\text{cm}^3\text{hydrogel}}{\text{g NaCl}/\text{cm}^3\text{ donor solution}}$). Finally, the salt permeability coefficient, P_s, was estimated from the measured diffusion and partition coefficients[7]:

$$P_s = D_s K_s \quad (8)$$

Contact angle measurements were performed to characterize the hydrophilicity of the copolymer hydrogel films, unmodified, and modified membranes. A Ramé-Hart goniometer with an environmental chamber was used to immerse the hydrogel films in water and perform pendant drop contact angle measurements using air bubbles and n-decane droplets. Droplet volume was approximately 1 μL.

Zeta potential was measured for PEG hydrogels using an Anton-Parr SurPASS Electrokinetic Analyzer. The electrolyte solution was 10 mM NaCl, and the pH was adjusted using 0.1 M HCl or NaOH solutions. Streaming potential was measured, and the data were interpreted using the Fairbrother-Mastin approximation. All hydrogel films were equilibrated in 10 mM NaCl before testing.

Task 4: Preparation and Characterization of Coated and Surface-Modified Membranes

AG RO membranes were coated with a hydrogel film using drawdown coating. First, AG membranes were soaked in DI water in a covered container overnight to remove glycerin added during the manufacturing process. Then, membrane samples were patted dry and taped to a silicon wafer. Tape was applied only to two opposite edges of the sample; taping all four sides would result in a hydrogel coating the same thickness as the tape. A Gardco Automatic Drawdown Machine (DP-8201, Paul N. Gardner Company, Inc., Pompano Beach, FL) with rod size 0 was used to apply a uniform layer of liquid prepolymer mixture at a rate of 2.5 cm/s to the RO membrane. The entire coating apparatus was enclosed in a glove box under a N$_2$ purge, with a 312 nm UV light attached. After

the liquid prepolymer mixture was applied to the RO membrane, it was exposed to UV light for 90s at an intensity of 3 mW/cm^2. Coated membranes were rinsed and soaked in DI water until used. For simplicity, only PEGDA and 50 molar copolymers were used to prepared coatings.

In addition to creating a dense coating layer, modification by grafting was also investigated. Surface modification was performed on commercial Dow FilmTec XLE RO membranes. Before modifications were made, membrane samples were soaked in 25%(v) isopropanol for twenty minutes, then rinsed in deionized water, to remove glycerin from the membrane. Poly(ethylene glycol) diglycidyl ether, commonly referred to as PEG diepoxide, was the main focus of chemical modification studies (cf., Figure 3). Membranes were treated with aqueous solutions of PEG diepoxide, where several PEG diepoxide chain lengths (n values in Figure 3, n = 5, 9, 14 and 23), and concentrations (0.1-15%(w)) were used[10].

$$H_2C\!\!-\!\!HC\!\!-\!\!H_2CO\!\!\left(\!\!-OCH_2CH_2-\!\!\right)_n\!\!OCH_2\!\!-\!\!CH\!\!-\!\!CH_2$$
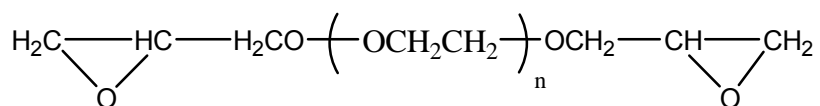
Figure 3. Chemical structure of poly(ethylene glycol) diglycidyl ether (PEG diepoxide) (n ≈ 5, 9, 14, or 23).

The dip coating procedure began with heating deionized water to 40°C using a Barnstead Electrothermal heating unit with stirrer. The appropriate amount of PEG diepoxide, allowed to equilibrate to room temperature, was then added to the water. The stirrer was turned off and the membrane was immediately immersed in the solution, to reduce the possible reaction time of PEG diepoxide and water. The membrane was left in the solution (keeping the temperature constant) for ten minutes. Finally, the membrane was removed from solution, triply rinsed in deionized water to remove unreacted PEG diepoxide, and stored in deionized water until use.

A top surface treatment method was also employed, in which the aqueous PEG diepoxide solution was allowed to contact only the top surface of the membrane. The procedure began with heating deionized water to 40°C using a Barnstead Electrothermal heating unit with stirrer. The appropriate amount of PEG diepoxide was then added to the water and the solution was shaken to thoroughly mix the PEG diepoxide and water. The solution was then poured into a casting ring placed on top of the membrane, to allow contact with only the top surface of the membrane. The membrane was left in contact with the solution for ten minutes. Finally, the membrane was triply rinsed in deionized water to remove unreacted PEG diepoxide, and stored in deionized water until use.

Attenuated total reflectance Fourier Transform Infrared Spectroscopy (ATR-FTIR) was performed on surface modified membranes using a Thermo Nicolet Nexus 470 FTIR (Madison, WI) with an Avatar Smart MIRacle ATR accessory

(Zinc Selenide crystal). Data were collected and analyzed using Omnic software. Spectra were collected using 128 scans at resolution of 4 cm^{-1} between 600 and 4000 cm^{-1}. Prior to analysis, samples were placed under vacuum overnight to remove excess water.

X-ray photoelectron spectroscopy (XPS) was used to detect membrane surface grafting. Samples are dried in a vacuum oven overnight before analysis. A PHI 5700 XPS (Physical Electronics, Chanhassen, MN) equipped with a monochromatic Al Kα$_{1,2}$ X-ray source performs a surface scan to detect carbon, nitrogen, and oxygen. Operating conditions are: 1x10^{-9} Torr chamber pressure; 14 kV; 250 W for the Al X-ray source. Steps are not taken to prevent the membrane from collecting charge; this creates a shift in XPS spectra. Therefore XPS spectra only provide relative amounts of C, N, and O on the surface and do not give insight into bond type.

Zeta potential was also measured on modified and unmodified RO membranes using the apparatus and methods described above. GE AG membranes were soaked in DI water prior to testing to remove glycerin. DOW membranes were soaked in 25% isopropanol for 20 minutes and then rinsed in DI water before testing.

Water flux measurements of coated and uncoated RO membranes in crossflow filtration were used with a flux resistance model to evaluate coating thickness. Pure water flux was measured after 4 hours of filtration, a time at which the water flux was steady. A flux resistance model was used to calculate the coating thickness:

$$J_{H_2O} = A_T(\Delta p) \tag{9}$$

where J_{H_2O} is the measured water flux, and Δp is the applied pressure. A_T is given as:

$$A_T = \left[\frac{1}{A_{RO}} + \frac{\ell}{P_{wPEG}} \right] \tag{10}$$

where A_{RO} is the RO membrane permeance, ℓ is the coating thickness, and P_{wPEG} is the hydrogel water permeability, previously measured for free-standing films.

Task 5: Characterization of Fouling and Separation Performance

Baseline water flux and NaCl rejection testing of commercial RO membranes was conducted in crossflow filtration using an industry-standard 2000 mg/L NaCl feed, prepared using deionized water from the Millipore system, and the optimum pressure and flowrate for each material, as specified by the manufacturer. Membranes were supplied on a roll, and several rotations of material were discarded before taking samples for testing. Feed pH was adjusted by addition

of NaHCO$_3$, HCl, or NaOH. The feed was either prefiltered using an activated carbon + particle filter, or unprefiltered, depending on the test conditions of the manufacturer.

Concentration polarization was studied in unmodified GE AG RO and Dow FilmTec XLE membranes. When membranes are subjected to feed solutions containing solutes such as salts, a boundary layer develops near the membrane surface in which the solute (e.g. NaCl) concentration ($c_{so(m)}$) is significantly higher than in the bulk feed solution (c_{so})[11]. Figure 4 is an illustration of the boundary layer formed near the membrane surface.
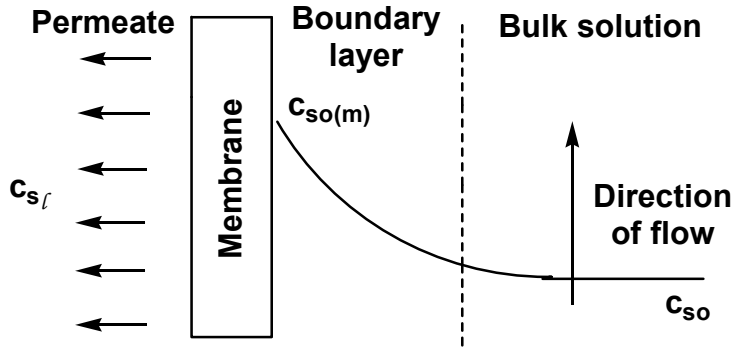
Figure 4. Boundary layer formation near the membrane surface.

Since it is impossible to measure concentration at the membrane surface ($c_{so(m)}$), the bulk concentration (c_{so}) is used to calculate observed rejection. The concentration polarization modulus, M, is a factor which can be used to correct the observed performance values obtained using bulk concentration, thereby obtaining the inherent material properties of the membrane, independent of polarization effects caused by the fluid dynamics of the system.

The concentration polarization level in our crossflow system was determined using a model based on the fact that the water permeability of a membrane is a material property and therefore independent of the feed[12]. The concentration polarization modulus, M, is given by this model as[12]:

$$M = \frac{\pi_{so(m)} - \pi_{s\ell}}{\pi_{so} - \pi_{s\ell}} = \frac{\Delta p}{\pi_{so} - \pi_{s\ell}} \times \left(1 - \frac{J_{w(NaCl)}}{J_{w(pw)}} \right) \qquad (11)$$

The osmotic pressure at the membrane surface, $\pi_{so(m)}$, is given by:

$$\pi_{so(m)} = \pi_{s\ell} + \Delta p \times \left(1 - \frac{J_{w(NaCl)}}{J_{w(pw)}} \right) \qquad (12)$$

where Δp is the applied transmembrane pressure, $\pi_{so(m)}$, $\pi_{s\ell}$, and π_{so} are the osmotic pressures at the membrane surface, in the permeate, and in the bulk feed, respectively, $J_{w(NaCl)}$ is the water flux in 2000 mg/L NaCl feed, and $J_{w(pw)}$ is the water flux in pure water feed. To determine the polarization level experimentally, pure water flux is measured ($J_{w(pw)}$), then 2000 mg/L NaCl is added to the feed and water flux ($J_{w(NaCl)}$) and bulk and permeate concentrations are measured. After the concentrations are converted to osmotic pressures (π_{so}, and $\pi_{s\ell}$), the polarization modulus and membrane surface salt concentration can be calculated. The actual salt rejection of a membrane is given by:

$$R_{actual} = \left(1 - \frac{\pi_{s\ell}}{\pi_{so(m)}}\right) \times 100\% \qquad (13)$$

where $\pi_{s\ell}$ and $\pi_{so(m)}$ are the salt concentrations in the permeate and at the membrane surface, respectively. The observed salt rejection is calculated using the bulk concentration (π_{so}) instead of the membrane surface concentration ($\pi_{so(m)}$), and is always lower than the actual salt rejection. Thus, the model allows simple calculation of the surface concentration, polarization modulus, and actual salt rejection from easily measured experimental quantities.

Fouling studies were also conducted in crossflow filtration mode as described above. Model foulants and emulsions, described above, were used, and rejection of organic carbon was measured using a Shimadzu TOC 5050A Total Organic Carbon Analyzer.

RESULTS AND DISCUSSION

Task 1: Emulsion Characterization

Two produced water emulsion samples from the southwest region of the United States were obtained and analyzed, one from a natural gas well and one from an oil well. A detailed analysis can be found in Appendix I. As expected, both samples contained a large amount of total dissolved solids. The oil well sample TDS was 230,000 mg/L, and the natural gas sample TDS was 16,000 mg/L. The largest component in each of these was sodium chloride. Calcium carbonate and sulfate were also found in significant amounts in each sample. Surprisingly, the natural gas sample had a higher total organic carbon count, 1650 mg/L, than the oil well, 106 mg/L, although the oil well sample contained more aromatic hydrocarbons such as benzene, toluene and phenol. The analysis also showed high levels of heterotropic bacteria, 470,000 MPN/L for the natural gas sample and 116,000 MPN/L for the oil well sample.

Although complex, this analysis was useful in the preparation of model emulsions. Knowing the major components and compositions of various

produced water samples allowed for the formulation of more realistic experimental conditions.

Using the above analysis as a starting point to select basic emulsion components, model emulsions for fouling tests were made using charged surfactants, NaCl, and *n*-decane or *n*-dodecane. An optical microscope was used to estimate the droplet size distribution and stability of a 150 ppm SDS and *n*-decane emulsion, prepared as detailed above. The emulsion contained 2000 mg/L NaCl, 15 ppm SDS, and 135 ppm decane, a 1:9 ratio of surfactant to oil. The emulsion was examined approximately one hour after blending, allowing for transport time between laboratories. Figure 5 shows a representative image of the emulsion.
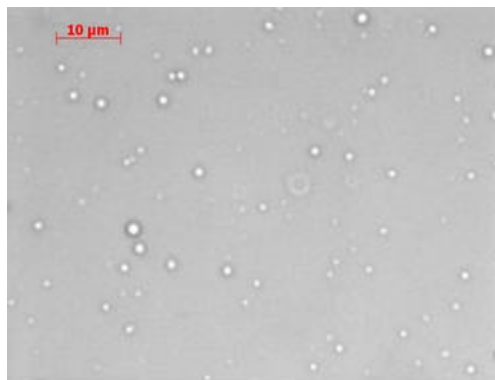
Figure 5. Microscopic image of oil emulsion.

One hour after blending the number average diameter, d_N, was 0.94 μm, and the volume average diameter, d_v, was 1.17 μm (see Eqs. 1 and 2, respectively). The PDI (Eq. 3) was 1.25, indicating droplet diameters to be fairly narrow in distribution. The same emulsion was examined 24 hours after blending. The d_N was 1.09 μm, d_v was 1.27 μm, and the PDI was 1.16.   Therefore, after 24 hours the droplets appeared to be slightly larger with an even narrower range of diameters. This change indicates the emulsion droplets are beginning to aggregate, but the differences seen in one day were not considered to be significant.

Task 2: Selection of Commercial Membrane Supports

GE AG, Dow XLE, and LE RO membranes are leading products in the RO market. Therefore, they are considered to be representative of the best of all commercially available membranes, and are logical candidates for use in this work.

Task 3: Synthesis and Characterization of Fouling Resistant Materials

Free-standing PEG hydrogel films were successfully synthesized. ATR-FTIR was used to gauge reaction conversion (data not shown here). Reaction of all copolymers was assumed to be complete.

Water transport properties of free standing PEG films were evaluated to determine the suitability of these materials as membrane coatings. Figure 6a presents water sorption as a function of comonomer content for each copolymer

series. PEGA copolymers exhibited the largest sorbed volume fraction of water, and HEA copolymers sorbed more water than a pure PEGDA hydrogel. The water volume fraction in AA copolymers was slightly higher than that of PEGDA, but changed little with comonomer content.

The observed water sorption behavior presumably stems from the monomer chemistry and crosslink density of each copolymer. Figure 6a clearly shows the influence of comonomer type on the copolymer water sorption. In general, water sorption increases with increasing comonomer chain length. For example, at 60 mol% comonomer, the lowest copolymer water uptake corresponds to the copolymer with the shortest chain, 60AA, and the highest water uptake corresponds to the copolymer with the longest chain, 60PEGA. Subsequently, the copolymer with the mid-length chain, 60HEA, has water uptake between that of 60AA and 60PEGA copolymers.
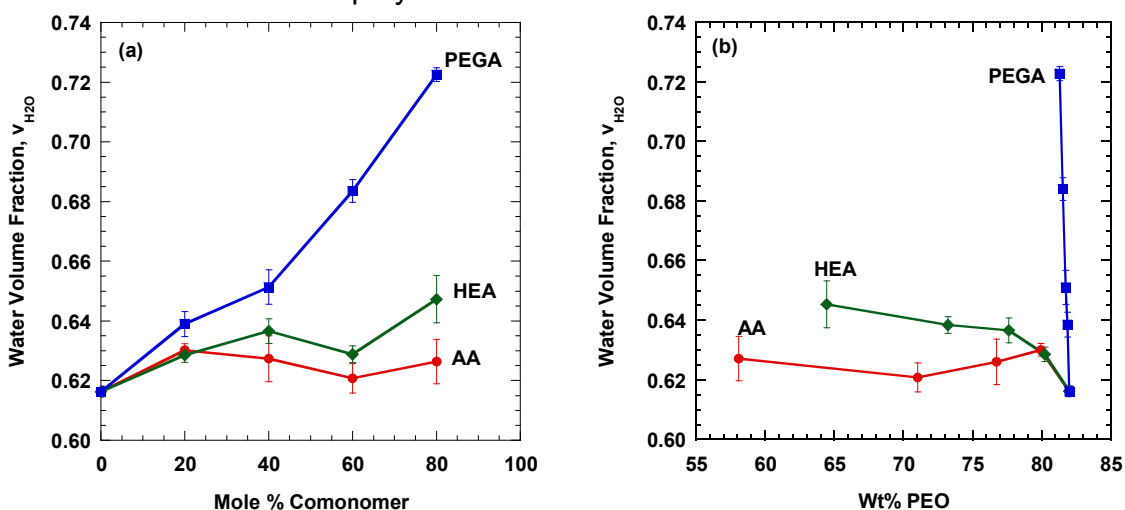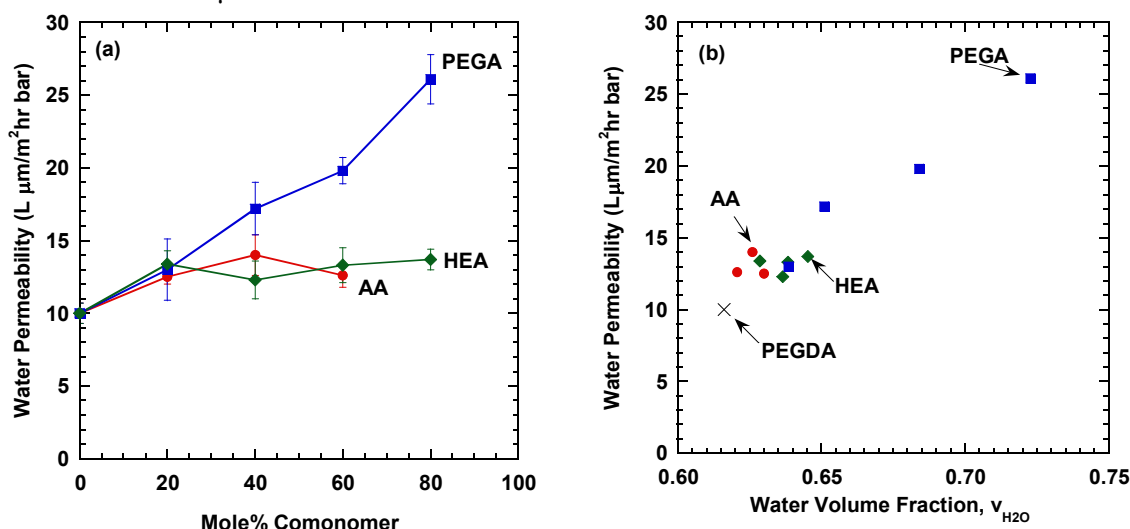

Figure 6. Hydrogel water volume fraction as a function of **(a)** copolymer composition and **(b)** PEO content.

Crosslink density can also influence water sorption behavior. Crosslink density decreases as monomer content increases. When all other factors are constant, decreasing crosslink density typically increases water uptake by giving the polymer network more mobility and freedom to swell[13]. However, even in the absence of crosslinks, swelling will only occur up to the solubility limit of water in the copolymer. In this regard, the PEO content of the copolymers might also influence water uptake because water has an affinity for EO units[14]. Even high molecular weight PEO is soluble in water at room temperature[15]. Figure 6b presents the sorbed water volume fraction as a function of PEO weight percent in each copolymer. PEGDA and PEGA are both approximately 82 wt% PEO, so PEO content remains constant for this series. Therefore, the increase in water volume fraction in PEGA copolymers can be solely attributed to the decrease in crosslink density with increasing PEGA content. Conversely, AA does not contain any PEO, and HEA is 38 wt% PEO, so in addition to changing the crosslink density, the chemistry changes significantly as comonomer content

increases. However, AA and HEA copolymer water volume fractions remain relatively constant over a range of chemical compositions and crosslink densities, indicating that the compositional changes appear to offset the effect of crosslink density on water volume fraction. One possibility is physical crosslinking, induced by the increased propensity of HEA and AA to participate in hydrogen bonding[16]. This physical crosslinking would restrain copolymer swelling, counterbalancing the effect of decreased chemical crosslinking.

Water permeability was determined as a function of copolymer composition from water flux measurements and Eq. 6. Water permeability was independent of pressure in the tested pressure range. As Figure 7a shows, trends in water permeability with respect to comonomer content are similar to trends in water sorption. That is, PEGA copolymers have the highest water permeability, and AA and HEA copolymer permeabilities are not strong functions of copolymer composition. These trends further underscore the importance of crosslink density and hydrophilic content on water transport properties. Water permeability for 80AA is not reported because the sample is phase-separated, meaning the sample is macroporous and transport does not occur in the same manner as it does in the non-phase-separated samples[17]. Water permeability for 80AA is in excess of 100 Lμm/m^{2}hr bar.


Figure 7. Copolymer water permeability as a function of **(a)** copolymer composition and **(b)** water volume fraction.

Figure 7b presents a correlation of water permeability with water volume fraction. In general, higher hydrogel water volume fraction leads to higher hydrogel water permeability, regardless of chemical composition.

NaCl uptake and transport properties of the free-standing PEG films were also measured. As shown in Figure 8, NaCl desorption behavior is largely consistent with that expected from Fickian diffusion models of solute release from a film of uniform thickness[7]. A short induction period was observed for many of the samples, indicated by the non-linear relationship between mass uptake and the

square root of time at the beginning of the experiment. This induction period may be partly attributed to delays in data collection, since the equipment used in this study could only collect data in 5 s intervals. Additionally, the induction period might be due to boundary layer effects at the beginning of the experiment, before the solution in which the sample was soaking became well-mixed. Such effects are known in the literature, and they were assumed to be small in this study.

The NaCl diffusion coefficient, D_s, for each copolymer was calculated from the slope of the linear portion of the desorption curve using Eq. 7, and the results are presented in Figure 9. NaCl diffusivity does not change significantly with changing AA or HEA content, but it does increase slightly with increasing PEGA content. Also, the difference in diffusivity between most of the copolymers is not significant, except for 80mole% copolymers, where 80PEGA is larger than 80AA. D_s of NaCl in pure water at 25°C is approximately 1.6×10^{-5} cm^2/s[18]. All of the measured values fall below this value. This result was expected because even though NaCl is in an aqueous solution, both NaCl and water must be transported through the hydrogel. Therefore, measured D_s values less than D_s of NaCl in pure water indicate that the NaCl is passing through the hydrogel network and not through any film defects.
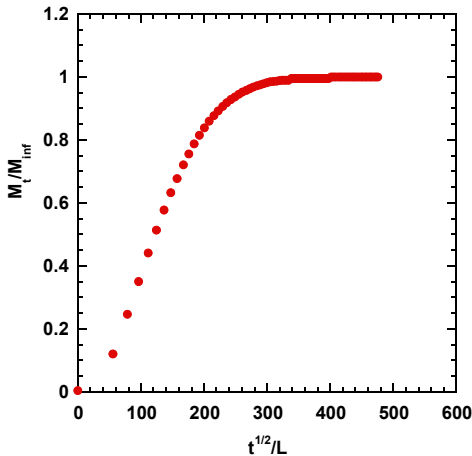
Figure 8. Example salt desorption curve used to calculate NaCl diffusion coefficient in a hydrogel.
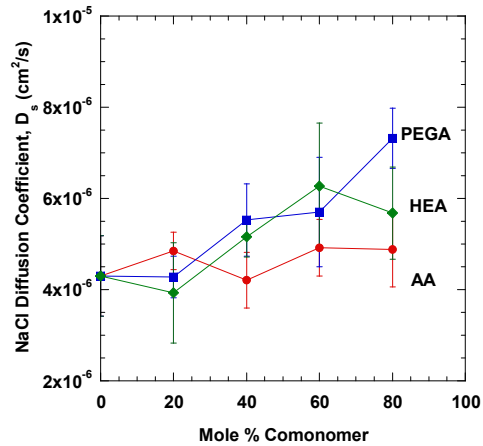
Figure 9. Diffusion coefficients of NaCl in hydrogel copolymers.

NaCl partition coefficients, K_s, were also determined from the desorption measurements, and the results are presented in Figure 10a. Trends in K_s with varying monomer content are reminiscent of the trends in water sorption for these materials. Like their water sorption behavior, AA and HEA copolymers show relatively little change in NaCl uptake with increasing comonomer content. However, PEGA copolymers show salt uptake increasing with increasing comonomer content, similar to its water sorption behavior. These results are reasonable since, to a first approximation, the amount of salt sorbed by the polymer network is often found to be sensitive to the water uptake. To determine if the NaCl concentration of the water sorbed by the hydrogel is the same as the

NaCl concentration in the surrounding water, the partition coefficient was modeled as follows[7]:

$$K_s = K_{polymer} \mathrm{v}_{polymer} + K_{H_2O} \mathrm{v}_{H_2O} \qquad (14)$$

where K_s is the measured NaCl partition coefficient, $K_{polymer}$ and K_{H_2O} are the partition coefficients of the polymer and water, respectively, and $\mathrm{v}_{polymer}$ and v_{H_2O} are the volume fractions of polymer and water, respectively, in the polymer. If NaCl is not sorbed by the polymer, i.e., if the polymer is impenetrable to NaCl, then $K_{polymer}$ would be zero. Also, K_{H_2O} is, by definition, one. In this case, Eq. 14 reduces to[7]:

$$K_s = \mathrm{v}_{H_2O} \qquad (15)$$

Therefore, the measured NaCl partition coefficients are plotted versus v_{H_2O}. As shown in Figure 10b, all of the measured partition coefficients fall below the line given by Eq. 15, so the hydrogels sorb more water than NaCl. These results indicate that the materials exhibit some solubility selectivity for water over NaCl.
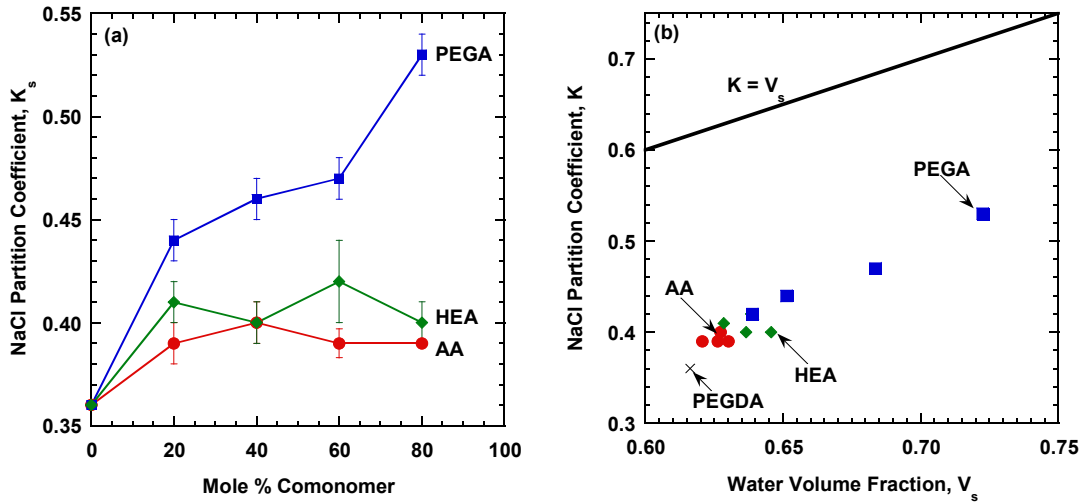
Figure 10. NaCl Partition coefficients as a function of **(a)** copolymer composition and **(b)** water volume fraction.

Finally, NaCl permeability coefficients were calculated using the measured D_s and K_s values along with Eq. 8. The results are presented in Figure 11. As seen with both the salt uptake and diffusion behavior, AA and HEA copolymer NaCl permeabilities are relatively constant for all comonomer contents. PEGA copolymer NaCl permeability increases with increasing comonomer content.
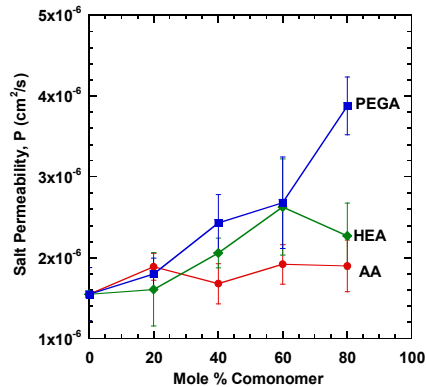
Figure 11. NaCl permeability as a function of copolymer composition.

Contact angles of the PEG-based films were measured using a pendant drop technique. The samples were immersed in DI water, and *n*-decane was used as the probe liquid. The reported angle was measured through the aqueous phase, so angles of 90° and greater represent hydrophobic surfaces, and angles less than 90° represent hydrophilic surfaces. The data are presented in Table 1. There is not a discernable trend relating contact angle to copolymer content or monomer type. Experimental error was large in some cases, which is a typical challenge of contact angle measurements[19].

Table 1. Oil-in-water pendant drop contact angles of hydrogel films

Sample	Contact Angle (^{0})
PEGDA	49 ± 2
20AA	56 ± 4
40AA	62 ± 7
60AA	54 ± 4
80AA	32 ± 3
20HEA	46 ± 3
40HEA	56 ± 8
60HEA	51 ± 1
80HEA	49 ± 4
20PEGA	48 ± 1
40PEGA	40 ± 3
60PEGA	37 ± 3
80PEGA	44 ± 4

Hydrogel zeta potentials were measured using films equilibrated in 10 mM NaCl before testing. As Table 2 demonstrates, at a given pH, all of the PEG films exhibit similar zeta potential values. In comparison, the zeta potential of the AG membrane is also listed. The PEG-based materials clearly have less charge at pH 7 than the AG membrane, a promising feature for potential coating materials. The isoelectric point of all the materials is also similar.

Table 2. Zeta potential at selected pH values

Sample	Zeta Potential, ζ (mV)		pH of IEP
	pH 3	pH 7	
PEGDA	1.0 ± 0.9	-2.2 ± 0.3	3.4
50AA	4.2 ± 1.1	-5.5 ± 0.4	3.8
50HEA	1.4 ± 0.4	-5.7 ± 0.3	3.8
50PEGA	4.1 ± 1.1	-4.3 ± 1.1	4.3
AG RO Membrane	9.0 ± 0.4	-39.5 ± 0.5	3.7

Task 4: Preparation and Characterization of Coated and Surface-Modified Membranes

Efforts to prepare coated RO membranes focused on drawdown coating methods. Previous work on spin-coated membranes showed inconsistent results between water flux measurements, calculated thicknesses, and SEM imaging. It was believed that water evaporated from the prepolymer solution during the spin coating process, changing the overall coating permeability. Since it is extremely difficult to quantify the amount of water that could evaporate during spin coating, and therefore, very difficult to know the coating permeability, drawdown coating was chosen to eliminate the effect of evaporation.

First, ATR-FTIR was done on a PEGDA-coated membrane to verify the existence of a coating layer. Figure 12a shows spectra of an uncoated membrane and a dense PEGDA film. Figure 12b, the spectrum of a PEGDA-coated RO membrane, clearly shows characteristic peaks from both spectra in Figure 12a. The peak at 1724 cm^{-1} in the PEGDA-coated spectrum represents the vibrations

of the C=O bond in the acrylate group of PEGDA. This peak is not observed in the uncoated membrane spectrum, but is prominent in the free-standing PEGDA spectrum. The presence of this peak confirms the presence of PEGDA on the membrane surface. Other spectra of PEGDA-coated membranes, not presented here, show varying intensity of the PEGDA peaks, with the polyamide signals always being dominant. These differences in the spectra indicate that either (1) the coating layer is non-uniform, and/or (2) the coating layer is quite thin.
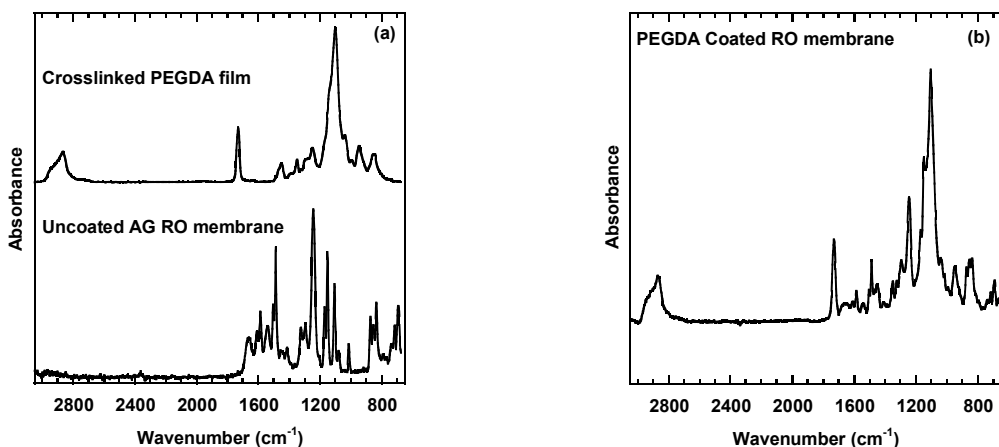
Figure 12. FTIR spectra of **(a)** an uncoated RO membrane, a free-standing PEGDA film, and **(b)** a PEGDA-coated membrane.

XPS was also done to detect PEGDA on the membrane surface. First, theoretical amounts of carbon and oxygen were calculated for PEGDA, based on the chemical structure given in Figure 2. Theoretical amounts of carbon, oxygen, and nitrogen were calculated for the polyamide, assuming the polyamide contained 100% trimesoyl chloride, as opposed to a mixture of trimesoyl and dimesoyl chloride, and also assuming that all three functional groups on the trimesoyl chloride were reacted. Three different samples were submitted for XPS analysis: (1) an uncoated AG membrane (polyamide), (2) an AG membrane coated with 100%PEGDA containing no water in the prepolymer mixture, and (2) an AG membrane coated with the standard PEGDA prepolymization mixture containing 60 wt% H_2O. The sample coated with PEGDA and no water was done to minimize shrinkage of the coating upon drying. All three samples were tested for O, N, C and S content. Sulfur content could be expected due to the underlying polysulfone layer. However, in all three samples, the sulfur signal was not distinguishable from the background noise, and is not reported here. Table 3 presents theoretical calculations and XPS results for the three submitted samples.

The measured composition for the AG membrane matches very closely to the predicted composition. However, both the PEGDA-coated membranes still show a significant amount of detectable nitrogen, indicating that the coating does not cover the entire membrane surface. Furthermore, the membrane coated with PEGDA and no water shows a smaller nitrogen signal than the one coated with PEGDA in 60wt% water, indicating that shrinkage is occurring, and that

techniques requiring complete drying of the coated membranes are not going to give an accurate picture of the coated membrane topology.

Table 3. XPS results for Uncoated and Coated Membranes.

Sample	Elemental Composition (Wt %)		
	O	N	C
Calculated PEGDA	60.0	0	40.0
Calculated Polyamide	18.3	13.0	68.7
AG RO Membrane	15.3	11.2	73.5
PEGDA-Coated 0 wt% H_2O	24.7	6.6	68.2
PEGDA-Coated 60 wt% H_2O	22.3	8.1	69.1

Next, membranes coated with different coating chemistries were tested in crossflow filtration at 225 psig, 0.8 gpm, and 25°C using water with 100 mg/L NaCl (to help stabilize pH) for 4 hours to collect the "pure" water flux. Then 2000 mg/L NaCl was added, and the samples were run for another 4 hours to collect salt water flux and rejection data. Membrane flux and rejection values are presented in Table 4. Coating thicknesses were calculated using the given data and Eqs. 5 and 6. The coating thicknesses appear to be between 1 to 2.5 microns, which was expected based on the coating rod size.

Table 4. Water flux, coating thickness, and salt rejection of uncoated and coated RO membranes

Sample	Pure Water Flux, J_w (LMH)	Coating Water Permeability ($L\mu m/m^2 hrbar$)	Coating Thickness, ℓ (μm)	Salt Water Flux, J_s (LMH)	NaCl Rejection (%)
AG RO Membrane	70.1 ± 4.2	NA	NA	61.1 ± 3.5	99.1 ± 0.5
PEGDA-Coated	40.1 ± 2.9	10.0 ± 0.7	1.5 ± 0.3	37.7 ± 2.9	99.3 ± 0.5
50AA-Coated	41.7 ± 4.1	12.9 ± 0.5	2.1 ± 0.7	40.3 ± 2.0	99.1 ± 0.1
50HEA-Coated	46.3 ± 0.9	12.1 ± 0.5	1.6 ± 0.1	42.7 ± 0.8	99.4 ± 0.1
50PEGA-Coated	44.8 ± 2.2	17.8 ± 0.3	2.4 ± 0.4	42.3 ± 2.2	99.2 ± 0.4

Attempts to use Eq. 11 to calculate concentration polarization modulus values for the coated membranes resulted in values less than one, which is not feasible in this testing scenario. Interestingly, the decline in water flux for the coated membranes in a 2000 mg/L NaCl feed does not correspond to that expected from the loss in driving force due to increased osmotic pressure in the feed. This behavior indicates that the membrane permeance does not remain constant, and therefore a different model must be used to calculate concentration polarization.

As expected, the average water fluxes of the copolymer-coated membranes were higher than the water flux of the PEGDA-coated membrane because of the higher copolymer water permeabilities. This result supports the use of a flux-resistance model to help predict coated membrane water flux. Differences in the

calculated coating layer thicknesses, despite the same coating conditions used for each sample, can be partly attributed to differences in swelling for the copolymers.

Zeta potential of coated membranes was also measured and compared to the zeta potentials of an uncoated membrane and of free-standing films. Figure 13 shows selected zeta potential data. Clearly, the AG membrane is more negatively-charged than the other samples in most of the tested pH range. Based on the zeta potential of the free-standing films (cf., Table 2), it was anticipated that the coated membranes would have a lesser charge. The coated membranes are less negatively-charged than the AG membrane, but their charge is not as low as that of a free-standing film. However, the lessened surface charge is a positive step towards creating a more fouling-resistant

Figure 13. Zeta potential as a function of pH for coated and uncoated membranes.

membrane, and even the small change in surface charge could result in better fouling behavior, especially in the presence of charged surfactants.

In addition to surface coating with a dense layer, surface modification by grafting was also studied. Direct chemical surface modification studies focused on poly(ethylene glycol) diglycidyl ether, or PEG diepoxide, as the grafting molecule. Dip coating has been the method of choice for surface grafting of PEG diepoxide to the XLE membrane surface. The extent of PEG diepoxide grafting appears to be directly proportional to the reaction time, as evidenced by lower pure water flux (i.e., more PEG surface coverage) of membranes dip coated for longer times. For example, XLE membranes dip coated with a 10%(w) solution of MW 200 PEG diepoxide at 40°C for 1 minute and 10 minutes had pure water fluxes of 75 and 45 L/(m^{2}h), respectively.

Several chain lengths of PEG diepoxide (n = 5, 9, 14 and 23, or molecular weights = 200, 400, 600 and 1000) have been grafted to the XLE membrane surface, using a reaction time of ten minutes. The molecular weight and concentration of PEG diepoxide strongly influence the resulting pure water flux of the modified XLE membrane, as seen in Figure 14. Figure 14 gives the pure water flux as a function of PEG diepoxide concentration. One interesting result seen in Figure 14 is that MW 400 PEG diepoxide gives grafted membranes with lower water flux than either MW 600 or 1000, which could indicate a change of attachment method (e.g., reaction at one chain end to form a brush versus reaction at both chain ends to form a loop) as the chain length of PEG diepoxide increases.
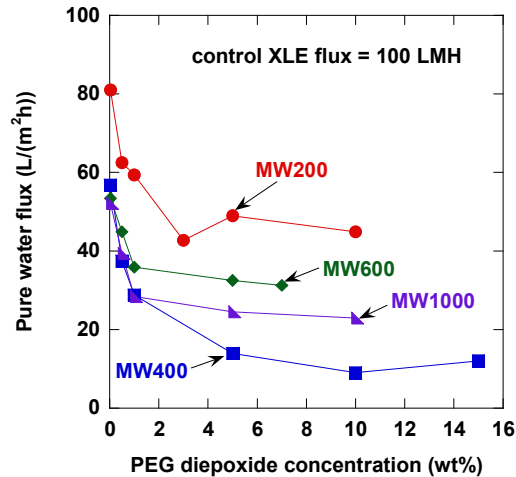
Figure 14. Pure water flux (dead end filtration, Δp = 150 psig) of XLE membranes dip coated (40°C, 10 minute reaction) with increasing concentrations of PEG diepoxide (molecular weights 200, 400, 600 and 1000).

The pure water flux data shown in Figure 14 suggest that low concentrations of PEG diepoxide will maximize water flux of the modified membranes. XLE membranes were then dip coated with several chain lengths (MW 200, 600, and 1000) and low concentrations (0.04-0.16 %(w)) of PEG diepoxide. Fluxes of the treated membranes and three controls (heated to 40°C in water) were measured using a 2000 ppm NaCl solution in a crossflow filtration test; results are given in Figure 15a. As PEG diepoxide chain length and concentration increased, flux decreased. The data presented in Figure 15b indicate that the PEG diepoxide-grafted membranes and the control membranes had comparable NaCl rejection capabilities.
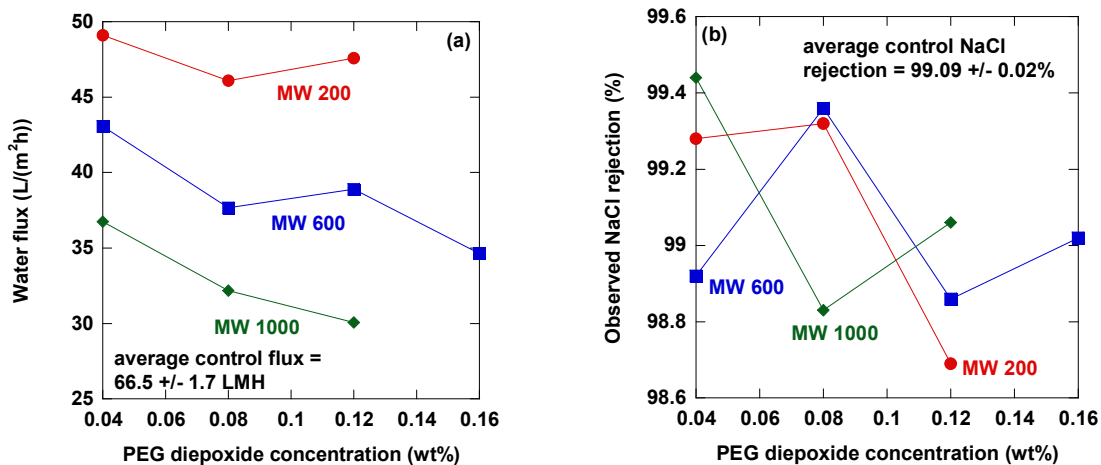
Figure 15. (a) Water flux and **(b)** NaCl rejection of XLE membranes grafted (40°C, 10 minute reaction) with PEG diepoxides of different chain length (MW 200, 600, and 1000) and concentrations.

Contact angle analysis was performed on GE AG RO membranes dip coated

with increasing concentrations of PEG diepoxide (MW 400). The results are given in Figure 16. The contact angle of a *n*-decane drop in water was measured; a smaller contact angle indicates less contact between the oil droplet and the membrane, or a more hydrophilic membrane surface. Results indicate that the most drastic decrease in contact angle, or increase in hydrophilicity, occurred for the lowest PEG diepoxide concentrations (0-2 vol%). This observation corroborates the decision to use low concentrations of PEG diepoxide for grafting.
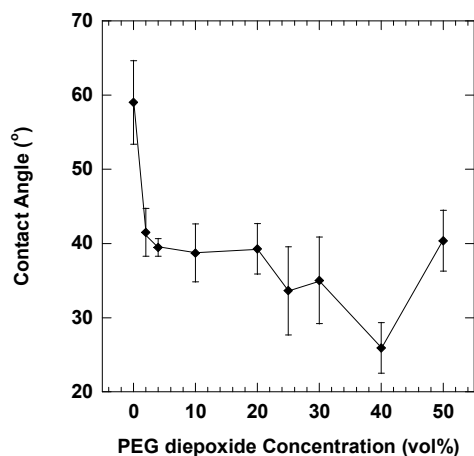
Figure 16. Decane in water contact angles for GE AG RO membranes dip coated with PEG diepoxide (n = 9, 40°C, 10 minute reaction).

Attempts were made to verify the presence of PEG diepoxide on the membrane surface after grafting to XLE membranes using X-ray photoelectron spectroscopy (XPS) and Fourier transform infrared spectroscopy (FTIR). XPS, a surface sensitive technique used to measure the elemental composition of the very top (~5 nm depth) of a surface, was used to determine the relative amounts of carbon, nitrogen, and oxygen present on the uppermost layer of the membrane. The O content of the membrane surface is expected to increase as the amount of PEG diepoxide grafted is increased, while the N content should decrease, since PEG diepoxide does not contain nitrogen. Table 5 shows that the O content of the membrane surface increased from 16.08% for an unmodified XLE membrane to 20.08% for a membrane grafted with 10%(w) MW 200 PEG diepoxide. The N content also decreases from 12.72% to 10.48%.

Table 5. XPS elemental analysis of XLE membranes grafted with MW 200 PEG diepoxide.

PEG diepoxide concentration (wt%)	C (%)	N (%)	O (%)
0	71.21	12.72	16.08
0.04	71.47	12.33	16.19
0.5	70.39	11.98	17.63
1	68.35	12.09	19.56
10	69.44	10.48	20.08

FTIR was also used to monitor the appearance of peaks associated with the ether C-O bonds of PEG diepoxide. Figure 17, the FTIR spectrum of MW 200 PEG diepoxide, shows that the largest peak is the ether peak centered around 1100 cm^{-1}. The spectra of XLE membranes grafted with increasing concentrations of MW 200 PEG diepoxide were subtracted from the spectrum of an unmodified XLE membrane, as seen in Figure 18. Differences in the 1100 cm^{-1} region indicated the extent of PEG diepoxide grafting to the membrane surface. As PEG diepoxide solution concentration increased, the extent of PEG diepoxide grafting also increased. However, Table 5 and Figure 18 both demonstrate the inability of XPS and FTIR to detect surface composition changes for very low PEG diepoxide concentrations (less than 0.5-1.0%(w)), and these low concentrations are the most promising for rendering modified membranes with high water flux.
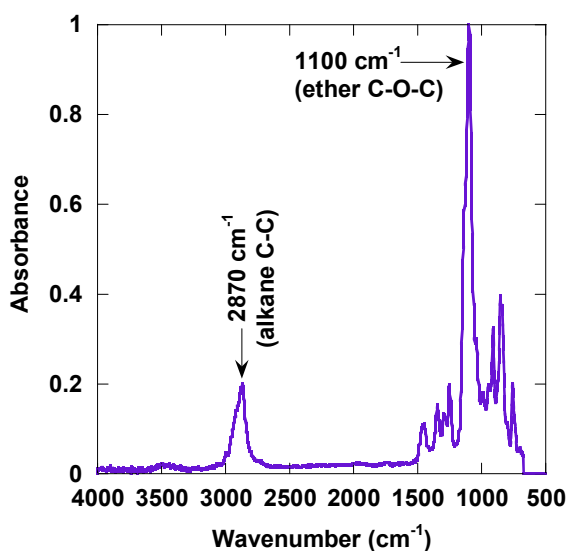
Figure 17. FTIR spectrum of MW 200 (n=4-5) PEG diepoxide.
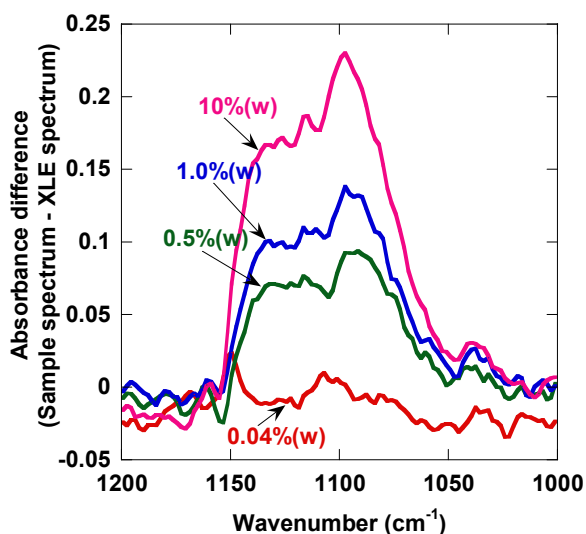
Figure 18. FTIR spectra of MW 200 PEG diepoxide-grafted XLEs subtracted from an unmodified XLE.

All initial work in the area of direct chemical surface modification was performed on commercial XLE RO membranes using a dip coating method. However, focus later turned to an alternate, top surface treatment method to maximize the water flux of the modified membranes. Since surface modification naturally reduces water flux (due to the additional mass transfer resistance of a grafting or coating layer), a method that minimizes this decrease was sought. The previous treatment method, dip coating, allowed the PEG diepoxide treatment solution to contact the entire membrane (both the nonwoven support layer as well as the active polyamide surface), resulting in adsorption of PEG diepoxide to the backing. An alternate method, in which the PEG diepoxide solution is only allowed to contact the active polyamide surface, was explored as a possible means of achieving higher water flux modified membranes.

In addition, modifications were performed on commercial NF90 membranes instead of XLE RO membranes. The water flux of the NF90 membrane is ~60% higher than that of the XLE membrane, and since they both share the same polyamide surface chemistry, reaction between PEG diepoxide and the membrane surface was expected regardless of which membrane was chosen for modification. Assuming that similar levels of grafting occur on the XLE and NF90 membranes, using the higher flux NF90 membrane for modification should result in higher flux modified membranes. However, use of the NF90 membrane was contingent on the ability of the PEG diepoxide to increase the NaCl rejection of the so-called "loose RO" NF90 nanofiltration membrane to a level comparable to the commercial LE and XLE RO membranes. To determine whether modification of NF90 membranes was feasible, the water flux and NaCl rejection of a series of PEG diepoxide-treated NF90 membranes was measured. Figure 19(a) shows the flux and rejection of NF90 membranes treated with MW 200 PEG diepoxide, while Figure 19(b) gives the flux and rejection fort NF90 membranes treated with MW 1000 PEG diepoxide. MW 200 PEG diepoxide was unable to increase the NaCl rejection of modified NF90 membranes above 97.3%, even using a 25%(w) treatment solution. It is possible that MW 200 PEG diepoxide simply does not have long enough chains to block NaCl passage through the loose NF90 membrane. However, as seen in Figure 19(b), the NaCl rejection of NF90 membranes treated with only 0.5%(w) MW 1000 PEG diepoxide was nearly 98.5%. Thus, MW 1000 PEG diepoxide is capable of increasing the NaCl

(a)   (b)
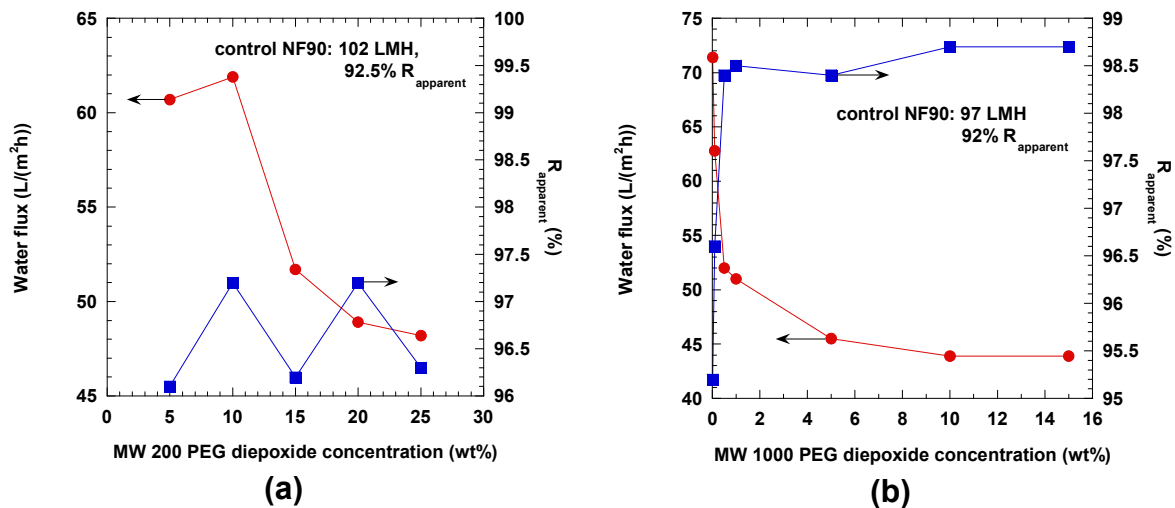
Figure 19. Water flux and apparent NaCl rejection of NF90 membranes modified with increasing concentrations of aqueous solutions of **(a)** MW 200 and **(b)** MW 1000 PEG diepoxide (Δp = 150 psi, flowrate = 1.0 gpm, T=24-25°C, feed run continuously through carbon and particle filter, feed pH = 6.9-7.0).

rejection of NF90 membranes to levels comparable to the LE or XLE RO membrane, making it a feasible choice for modification of NF90 membranes. Fouling studies were then conducted on NF90 membranes treated with 1-15%(w) MW 1000 PEG diepoxide solutions.

Surface characterization of NF90 membranes top surface-treated with MW 1000 PEG diepoxide was performed. Surface graft density ($\mu g/cm^2$) was measured

with a Rubotherm magnetic suspension balance capable of reading micrograms. Figure 20 shows that as the concentration of the aqueous PEG diepoxide solution is increased, the surface graft density increases. This trend is also supported by the water flux data in Figure 19b. Water flux decreases as the treatment solution concentration is increased, indicating more PEG diepoxide grafts to the membrane surface.
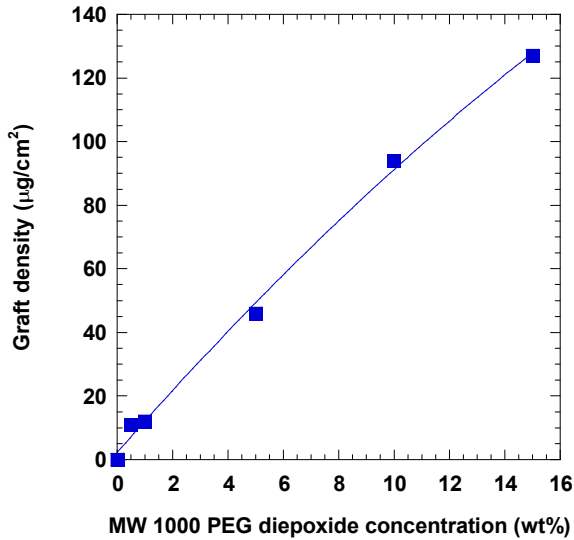
Figure 20. Surface graft density as a function of concentration of aqueous PEG diepoxide solution used for top surface-treatment of NF90 membranes.
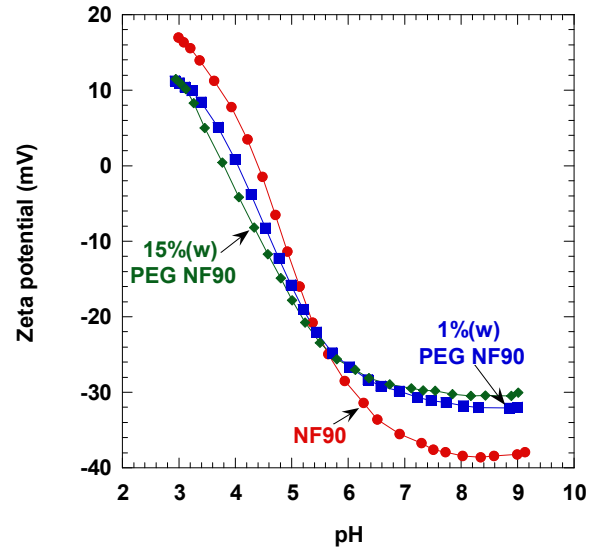
Figure 21. Zeta potential as a function of pH for NF90 membranes treated on their top surfaces with 1 and 15%(w) MW 1000 PEG diepoxide.

Zeta potential of the top surface-treated NF90 membranes was also measured. Figure 21 shows the zeta potential as a function of pH for NF90 membranes treated with 1 and 15%(w) aqueous solutions of MW 1000 PEG diepoxide. Their behavior is compared to that of an unmodified NF90 membrane, and a slight decrease in magnitude of surface charge is observable for the treated NF90 membranes. Thus, PEG diepoxide treatment of NF90 membranes decreases the magnitude of their negative surface charge in the normal pH range of testing (pH 7-8). The addition of PEG to the membrane surface, along with the decrease in surface charge, could improve the fouling resistance of these modified membranes over that of the unmodified commercial materials.

Task 5: Characterization of Fouling and Separation Performance

Before testing coated and grafted RO membranes, the water flux and NaCl rejection of unmodified RO membranes had to be determined. Obtaining water flux and NaCl rejection values (in industry-standard 2000 mg/L NaCl) of commercial RO membranes in agreement with the manufacturer's specifications proved difficult. Systematic adjustments were made to the crossflow apparatus and to the operating procedures to bring tested values into agreement with the manufacturers' values.

The first major roadblock to obtaining manufacturer-specified membrane performance parameters was the inability to maintain constant flux in the crossflow filtration test system. This problem was solved by the addition of a carbon + particle prefilter, which prevents biofouling due to naturally occurring biological growth in the feed tank over time, as well as particulate fouling due to fine contaminants present in the feed water. As seen in Figure 22, the flux of XLE membranes in pure water and 2000 mg/L NaCl feeds was steady over several days when the feed was continuously run through the prefilter. At the end of each run, 20 ppm dodecyltrimethylammonium bromide (DTAB) was added to the feed to measure the performance of XLE membranes subjected to this harsh foulant. In both runs, membrane flux decreased by 75% after addition of the foulant. Thus, the same steep initial flux decline as previously reported on AG membranes exposed to DTAB was also noted with XLE membranes.
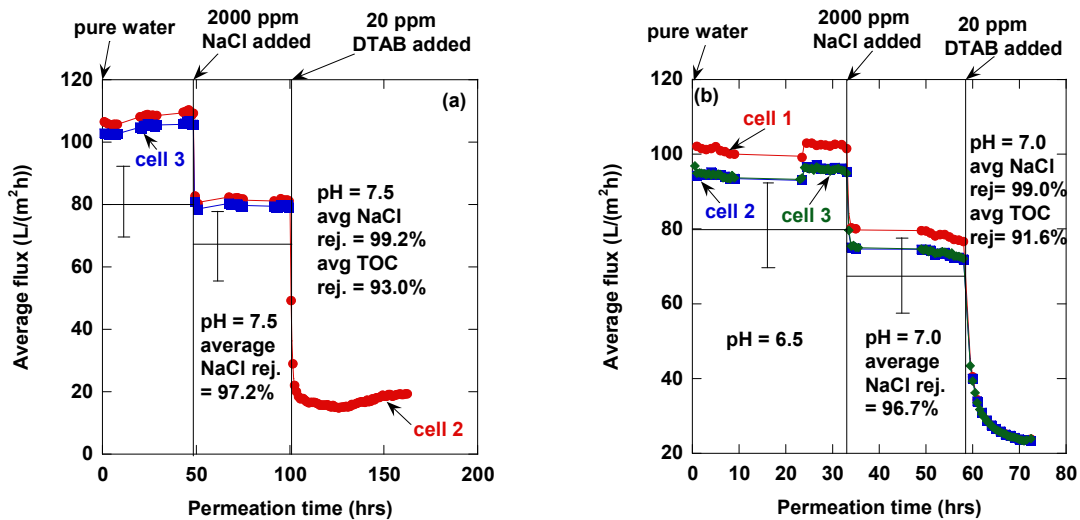
Figure 22. Crossflow filtration performance of unmodified XLE membranes. Cell numbers refer to order in which feed flows through membrane test cells. In run **(a)**, only two cells were used in series, while in run **(b)**, three cells were used in series.

Although the membrane flux was steady after installation of the carbon + particle pre-filter, the target flux and rejection values for XLE membranes still were not achieved. Vertical bars in Figure 22 indicate the expected flux range for XLE membranes subjected to pure water and 2000 ppm NaCl feeds. Experimental fluxes were slightly high, and observed NaCl rejection values were lower than expected (expected observed rejection is >98%), which suggested that leaks may be allowing a small portion of feed to bypass the membranes and mix with the RO permeate. However, leak testing using 1000 ppm $MgSO_4$ feed and XLE membranes (which should completely reject this salt) showed $MgSO_4$ rejection greater than 99.5%, indicating that leaks were not the cause of the high flux and low rejection. Thus, other possible explanations were sought for this behavior.

One variable which was thought to potentially affect membrane performance was the feed pH. The effect of feed pH on observed NaCl rejection of XLE and GE AG membranes was determined by measuring the rejection at several pH values

(pH was adjusted with dilute HCl or NaOH). The pH was alternated between acidic and basic values to ensure that any observed changes in rejection were due to the feed pH and not to damage caused to the membranes by acidifying or basifying the feed. Water flux was also monitored to determine the effect of feed pH on both membrane performance parameters. Figure 23a shows that observed NaCl rejection is a strong function of feed pH in the range 3-10. Rejection decreases significantly if the feed pH is lower than the pKa of the carboxylic acid and amine groups on the membrane surface (pKa~5). Figure 23b focuses on a narrower pH range (5-9), and demonstrates that observed rejection increases linearly with feed pH in this range, while water flux is independent of feed pH. Thus, feed pH appears to be a feasible cause of the lower than expected observed NaCl rejection values. Figure 23c presents flux and rejection data as a function of pH for the GE AG membrane. In general, the trends are the same for the AG and XLE membranes, although the AG membrane experiences less of a drop in rejection at lower pH values. The similar behavior between the two membranes was expected because of their similar chemical structures.
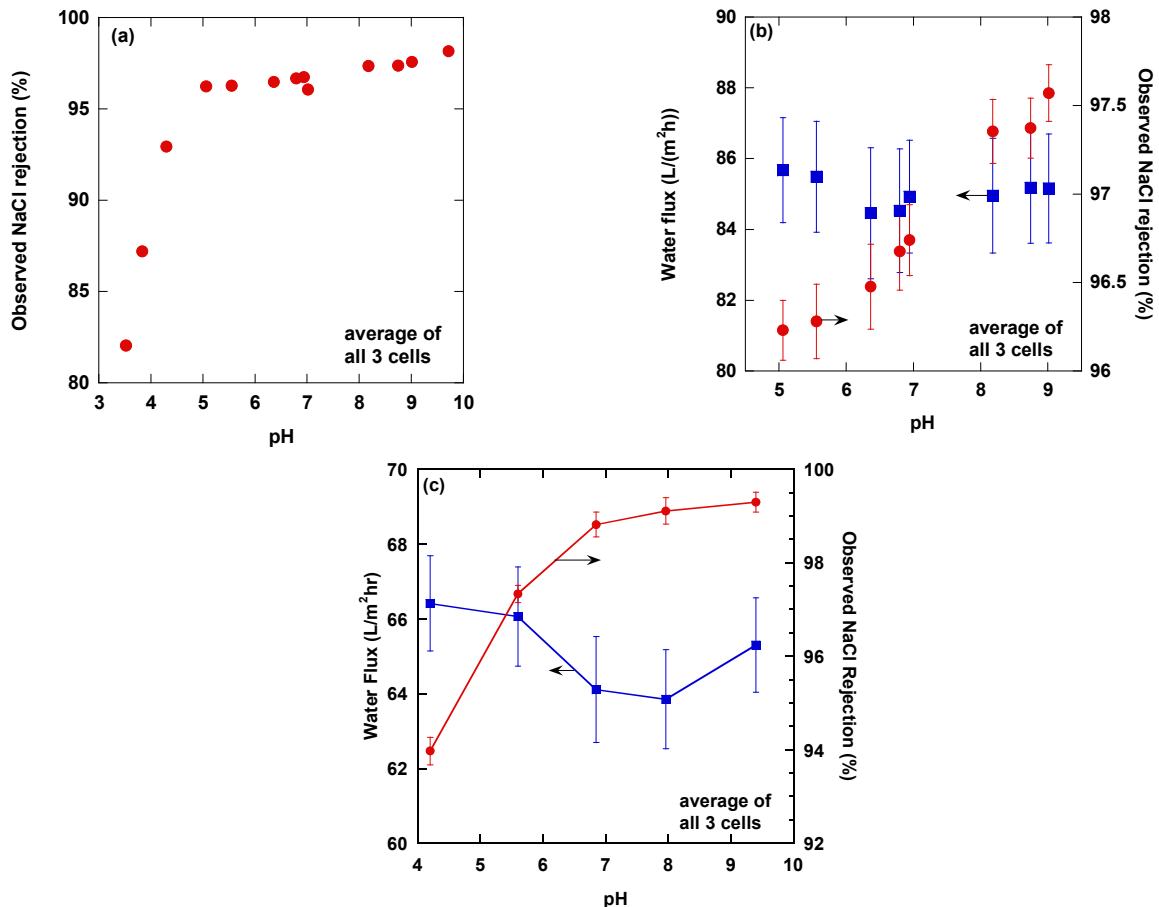
Figure 23. (a) Observed NaCl rejection as a function of feed pH in the range 3-10 and **(b)** water flux and observed NaCl rejection as a function of feed pH (XLE membranes, 2000 ppm NaCl, Δp = 150 psig, feed flowrate = 1.0 gpm, 25°C, feed run through carbon/particle prefilter). **(c)** Observed NaCl rejection and water flux as a function of feed pH for GE AG membrane (2000 ppm NaCl, Δp = 225 psig, feed flowrate = 0.5 gpm, 25°C, feed run through carbon/particle prefilter).

The water flux in Figure 23b is constant but is still nearly 10 L/(m^{2}h) above the target range given by the manufacturer (56 – 76 L/(m^{2}h)). The carbon/particle filter itself was then hypothesized to be the cause of the higher than expected water flux. Prefiltering the feed gives very stable water flux since any contaminants (biological and particulate) are continuously removed from the feed. However, tiny defects inherent to all RO membranes cannot be "patched" with naturally occurring feed water contaminants if the feed is prefiltered to an ultrapure state, resulting in higher water flux and lower NaCl rejection. Unprefiltered feed water may contain particulate matter and biogrowth, contaminants which can plug these surface defects, resulting in lower water flux and higher salt rejection.

A series of experiments was then performed to determine the effects of feed pH and prefiltration on membrane performance. Pure water flux was measured before adding the 2000 ppm NaCl, so that the observed rejection values could be corrected for concentration polarization using the model discussed in the experimental section. The water flux in pure water and 2000 ppm NaCl, along with the bulk permeate NaCl concentration, were used in Eqs. 12 and 13 to find the actual NaCl rejection. Figure 24a shows the effect of feed pH (6.0 vs. 7.9) on the water flux and actual NaCl rejection of XLE membranes, using unprefiltered feed water for both experiments. Although water flux is fairly unaffected by feed pH, rejection is much higher at the higher feed pH value. Figure 24b shows the effect of prefiltration (at pH 7.8-7.9) on XLE performance. Significant differences in flux and rejection are seen for unprefiltered versus prefiltered feeds. Prefiltered feed water leads to high, nearly constant water flux and only a slight increase in NaCl rejection over 24 hours. Membranes subjected to unprefiltered feeds show lower water flux and higher NaCl rejection than those subjected to continuously prefiltered feeds. In addition, membranes tested in unprefiltered feed show a much stronger dependence of flux and rejection on time, as flux declines steadily over 24 hours, and rejection increases steadily (3x more increase in rejection (0.6% vs. 0.2%) for membranes tested in unprefiltered feed). Prefiltration of the feed could explain both higher water flux and lower rejection.
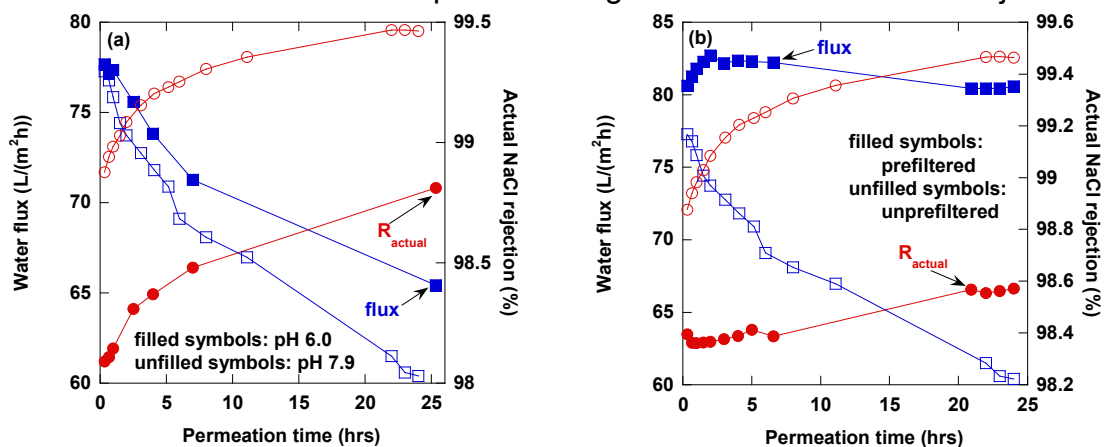
Figure 24. Water flux and NaCl rejection of XLE membranes versus time (2000 ppm NaCl, Δp = 150 psig, feed flowrate = 1.0 gpm, 25°C), demonstrating the effects of **(a)** feed pH (unprefiltered feed) and **(b)** prefiltration of the feed (pH 7.8-7.9) on membrane performance.

Once the effects of these two important variables, feed pH and prefiltration, were determined, the precise conditions under which the manufacturer obtains its specified performance values were used to test the membranes. The manufacturer of the XLE and LE membranes tests their membranes at pH 8 using unprefiltered feed water. Figures 25a and b show the water flux and NaCl rejection (observed and actual) of the LE and XLE membranes, respectively, during the course of a 24 hour crossflow experiment run at 150 psig and a flowrate of 1.0 gpm (pressure and flowrate chosen according to the manufacturer's optimums for these membranes). The feed is unprefiltered and buffered to pH 7.9 using $NaHCO_3$, to mimic the naturally occurring carbonate absorption from air into water. The flux of pure water (containing 100 ppm NaCl to stabilize pH) was measured after 20 minutes of operation (for use in concentration polarization calculations), then the balance of 2000 ppm NaCl was added and flux and rejection were monitored for 24 hours. Water flux declined steadily with time and rejection increased markedly during the 24 hour run, as expected with the unprefiltered feed water. Perhaps this explains the manufacturer's reasoning for taking performance values after only 20 minutes, before the effects of fouling have time to materialize. Table 6 compares the water flux and actual NaCl rejection values measured for each of the membranes in our laboratory to their manufacturer's specifications (time of measurement chosen to match manufacturer's practice). Although the water flux of the LE membrane is slightly above its target range, the water flux of the XLE membrane and both membranes' actual NaCl rejections match the manufacturer's specifications.
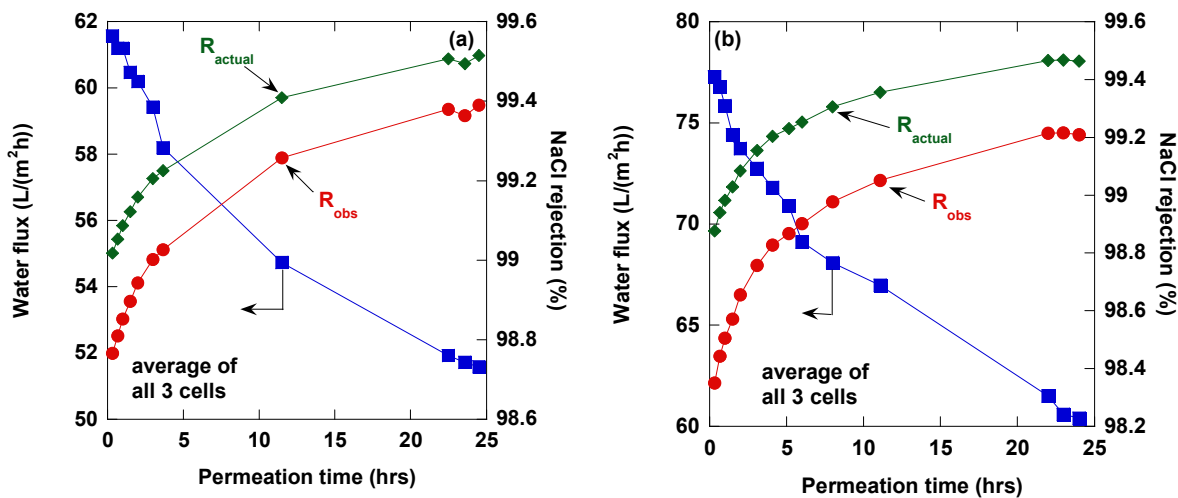
Figure 25. Water flux and NaCl rejection of unmodified **(a)** LE and **(b)** XLE membranes (2000 ppm NaCl, pH 7.9, unprefiltered, Δp = 150 psig, feed flowrate = 1.0 gpm, 25°C).

Table 6. Comparison of membrane performance values obtained in our laboratory to manufacturer's specifications at same testing conditions.

Membrane	Time (min)	Water flux (L/m²h)	Manufacturer's specified water flux (L/(m²h)	R_{actual} (%)	Manufacturer's specified R_{actual} (%)
AG[a]	60	67.3 ± 1.3	50 (40-65)	98.5 ± 0.4	98-99
LE[b]	20	61.6 ± 0.7	49 (42-56)	99.0 ± 0.3	99.0-99.3
XLE[c]	20	77.3 ± 2.0	66 (56-76)	98.9 ± 0.1	98.0-99.0

[a] Δp = 225 psig, feed flowrate = 0.5 gpm, 25°C, prefiltered feed, pH 7
[b,c] Δp = 150 psig, feed flowrate = 1.0 gpm, 25°C, unprefiltered feed, pH 7.9

The effects of feed flowrate on polarization modulus and actual (true) NaCl rejection of the XLE and AG membranes (at their manufacturer-specified optimal pressures, 150 psig for the XLE and 225 psig for the AG) were also determined using the concentration polarization model discussed above. Feed was continuously filtered through the carbon/particle prefilter to ensure the polarization was not affected by membrane fouling. Figure 26a shows the observed salt rejection, polarization modulus, and actual salt rejection as a function of flowrate for the XLE membrane. The observed salt rejection increases from 97.2 to 98.3% and the polarization modulus decreases from 1.65 to 1.2 as flowrate is increased from 0.3 to 1.0 gallons per minute. As flowrate increases, the feed is circulated across the membranes faster so less salt builds up at the membrane surface (i.e., lower polarization modulus). Also, since salt flux is proportional to salt concentration, lower surface concentration corresponds to less salt transport through the membrane, or higher salt rejection. Similar behavior was observed for the AG membranes, as shown in Figure 26b. Both experiments showed similar concentration polarization modulus values, further supporting the assumption that modulus values depend more on the fluid dynamics of the experimental system than on the membrane itself.
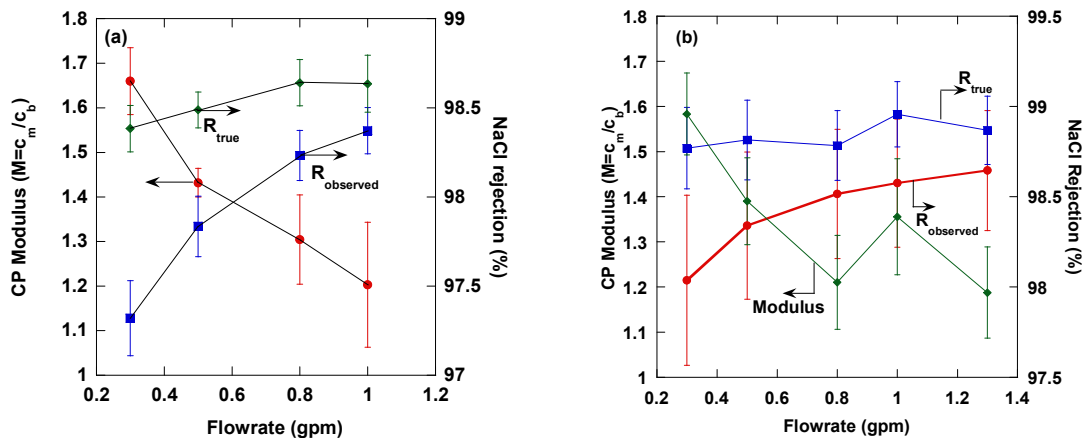
Figure 26. Observed salt rejection, concentration polarization modulus, and actual salt rejection at several flowrates for **(a)** the XLE membrane at 150 psig and **(b)** the AG membrane at 225 psig.

After being able to thoroughly understand the baseline behavior of unmodified, commercial RO membranes, focus turned to evaluating the fouling behavior of coated and grafted membranes. First, the fouling resistance of coated membranes in the presence of a cationic surfactant was tested. This was done by adding 200 ppm DTAB to the feed solution after salt water flux and rejection data were collected. Water flux was monitored for 24 hours after the addition of DTAB, and salt rejection and TOC rejection were collected at the end of the testing period. Figure 27 shows the water flux of an uncoated AG membrane and two PEGDA-coated AG membranes in the presence of 200 ppm DTAB feed. Interestingly, the fouling occurs immediately, with the flux for all three membrane samples dropping almost instantaneously, but then remaining relatively constant for the following 24 hours. This behavior was seen for all coated and uncoated membranes.
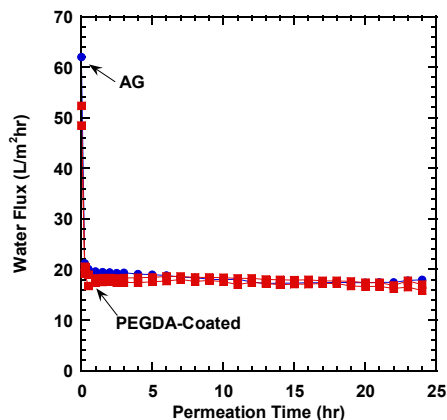
Figure 27. Fouling with 200 ppm DTAB in 2000 mg/L NaCl at pH ~ 7.

Table 7 gives the initial flux (i.e., the flux in the 2000 mg/L NaCl feed), the flux after 24 hours of DTAB exposure, and the flux decline of uncoated and coated membranes. The uncoated AG membrane shows the largest decline in water flux, with the final flux being only 30% of the original value. This behavior was expected due to the residual negative charge the RO membrane is known to have. It was also anticipated that the coated membranes would experience less fouling than the uncoated membranes, due theoretically, to the more neutrally-charged PEG-based coatings. Interestingly, the flux decline was loosely correlated with the pendant chain length of the copolymers. The 50AA copolymer, with the shortest pendant chain, had the least flux decline, followed by the 50HEA, 50PEGA, and PEGDA coatings. The salt rejection for all samples was minimum of 98.5%, well within the manufacturer specifications. TOC rejection for all samples was also greater than 98%, with many samples having near 100% TOC rejection.

Table 7. Summary of DTAB fouling for uncoated and coated membranes.

Sample	Salt Water Flux, J_s (LMH)	Flux with DTAB, J_D (LMH)	Flux Decline (J_s/J_D)
AG RO Membrane	62.1 ± 2.9	18.3 ± 1.1	0.30 ± 0.03
PEGDA-Coated	49.6 ± 1.2	16.4 ± 0.8	0.33 ± 0.03
50AA-Coated	41.7 ± 1.3	18.4 ± 0.4	0.44 ± 0.01
50HEA-Coated	42.7 ± 0.8	16.2 ± 0.7	0.38 ± 0.01
50PEGA-Coated	42.7 ± 1.6	15.4 ± 1.2	0.36 ± 0.04

After testing fouling with only DTAB, the uncoated and coated membranes were tested with an oily water feed in crossflow filtration. An emulsion containing 135 ppm decane, 15 ppm DTAB, and 2000 mg/L NaCl was added. The flux was monitored for 24 hours. The results for each polymer coating are shown in Figure 28a-d. In all four cases, the coated membranes maintain more of their water flux than the uncoated membrane. The PEGDA coating appears to maintain most of its initial water flux, having the highest flux after 24 hours.
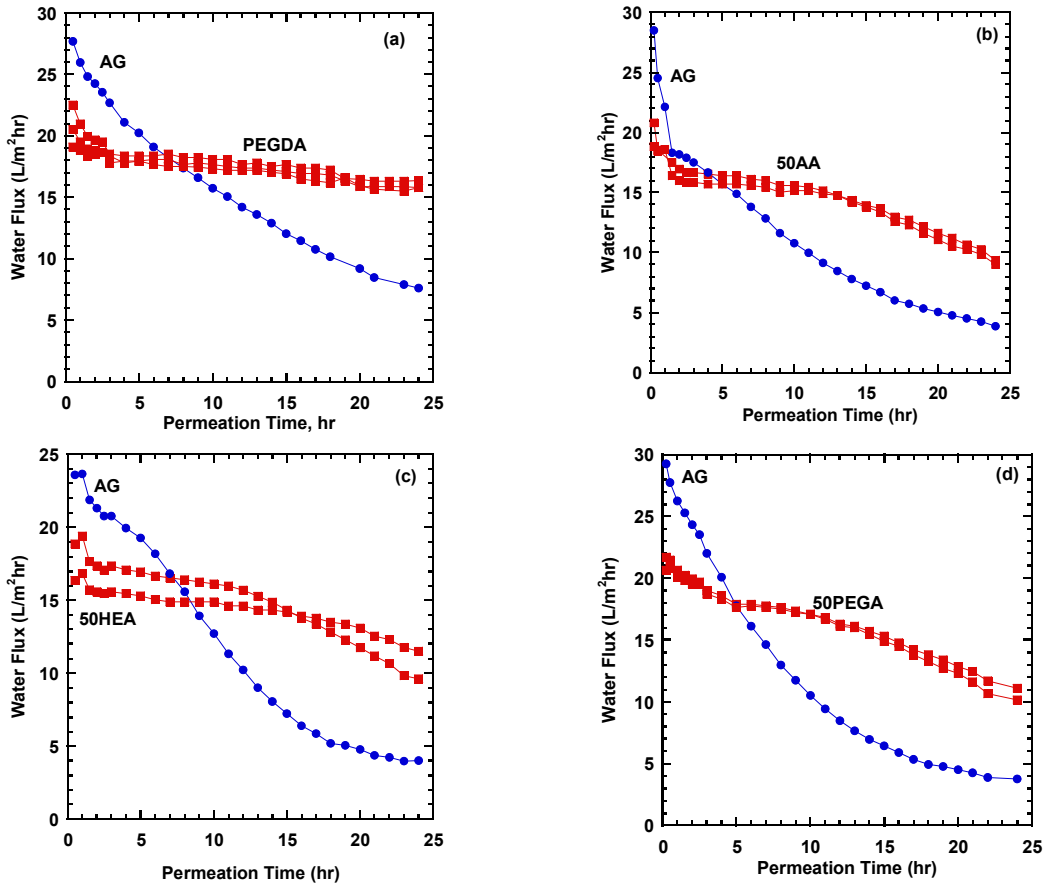
Figure 28. DTAB/Decane fouling for **(a)** PEGDA-coated **(b)** 50AA-coated **(c)** 50HEA-coated **(d)** 50PEGA-coated RO membranes. An uncoated membrane is also shown in each plot.

It is important to note the contribution of oil to the fouling mechanism. Previously, it was shown that the surfactant itself immediately fouls the membrane, with no further flux decline. However, in these oily emulsions, a continuous decline in water flux is seen. One can conclude that the initial starting point of the water flux can be attributed to the surfactant, but the subsequent fouling is due more to the oil.

Finally, the fouling resistance in the presence of an anionic surfactant, SDS, was tested on an uncoated membrane and PEGDA-coated membranes. It was

anticipated that the uncoated membrane would not experience fouling because the surface is negatively charged. The electrostatic repulsion between the negatively-charged surface and the negatively-charged surfactant should prevent fouling from occurring. Also, the coated membranes, having a lesser charge, but also a hydrophilic surface to prevent adsorption by the hydrophobic surfactant tail, should not experience fouling. Indeed, Figure 29a shows little to no flux decline over 24 hours in the presence of 200 ppm SDS.

However, the fouling behavior is drastically different in the presence of oil. An emulsion with 135 ppm decane, 15 ppm SDS, and 2000 mg/L NaCl was tested in crossflow filtration. Figure 29b shows the fouling of both the uncoated and coated membranes. Again, this data highlights the different roles of oil and surfactant in the fouling phenomena. The initial water flux for the uncoated AG membrane is much higher in the presence of decane/SDS, than in the presence of decane/DTAB. This behavior is consistent with that seen with surfactant alone. However, even though the initial water flux is higher, the uncoated membrane still experiences fouling in the decane/SDS emulsion, further highlighting the impact of oil on membrane fouling. Surprisingly, PEGDA-coated membranes also foul in the presence of decane/SDS, in stark contrast to its fouling resistance in decane/DTAB. This behavior indicates that pure electrostatic arguments are not sufficient to predict the fouling behavior of charged materials, and more work must be done to elucidate other important variables.
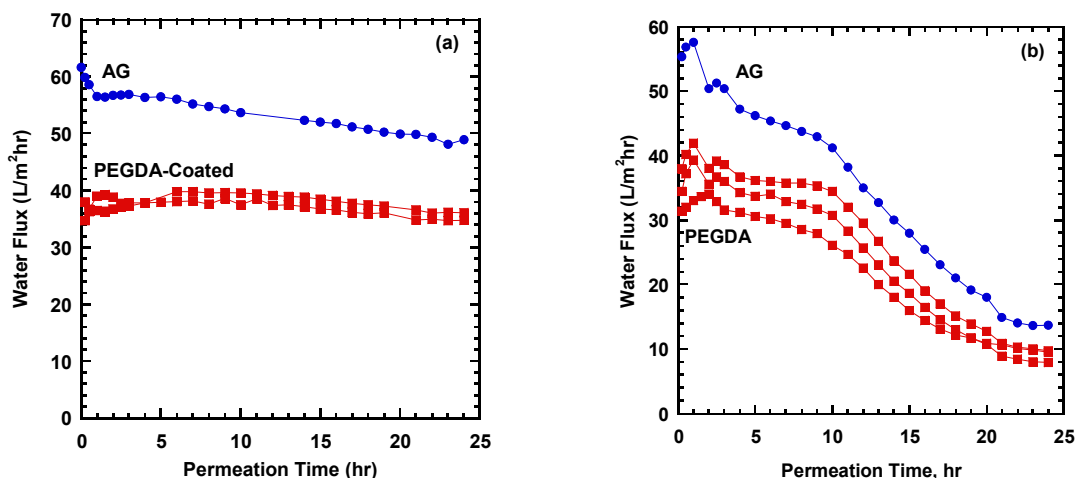
Figure 29. Fouling with **(a)** 200 ppm SDS in 2000 mg/L NaCl and **(b)**15 ppm SDS, 135 ppm decane, and 2000 mg/L NaCl.

Several crossflow fouling studies were performed on XLE and AG membranes grafted with various PEG compositions. The fouling performance of XLE membranes grafted with MW 600 PEG diepoxide was studied and compared to two control membranes: the XLE (heated to 40°C in water) and LE (not heated) membranes. The lower flux membrane (LE) was chosen because its flux in 2000 ppm NaCl solution is comparable to the flux exhibited by the MW 600 PEG diepoxide-treated XLE membranes. Therefore, a better comparison could be

made of their fouling performance. Two samples of each control membrane were tested. Two concentrations of MW 600 PEG diepoxide were used in the fouling study: 0.04 %(w) and 0.12%(w). Three membranes were made with each concentration. Also, an attempt was made to treat only the top surface of two 0.12%(w) PEG diepoxide-grafted membranes, since all previous treatments had been done by submerging the membrane in the PEG diepoxide solution. The flux was measured for a 2000 ppm NaCl solution, then a 25 ppm dodecane/25 ppm SLS emulsion was added, and the flux was monitored over the next two hours. Results are illustrated in Figure 30a. Although the initial fluxes of the treated XLE membranes were only half that of the control XLE membrane, the control membrane showed a significant amount of fouling, while the treated membranes did not experience any fouling. The treated XLE membranes also showed better fouling resistance than the control LE membranes chosen for their comparable initial flux. Salt rejection was also monitored as a function of time, as seen in Figure 30b. The PEG diepoxide-treated XLE membranes had the highest rejections. Interestingly, the flux and rejection of the top surface-treated membranes were almost identical to those of the submerged membranes (0.12 wt% MW 600 PEG diepoxide).
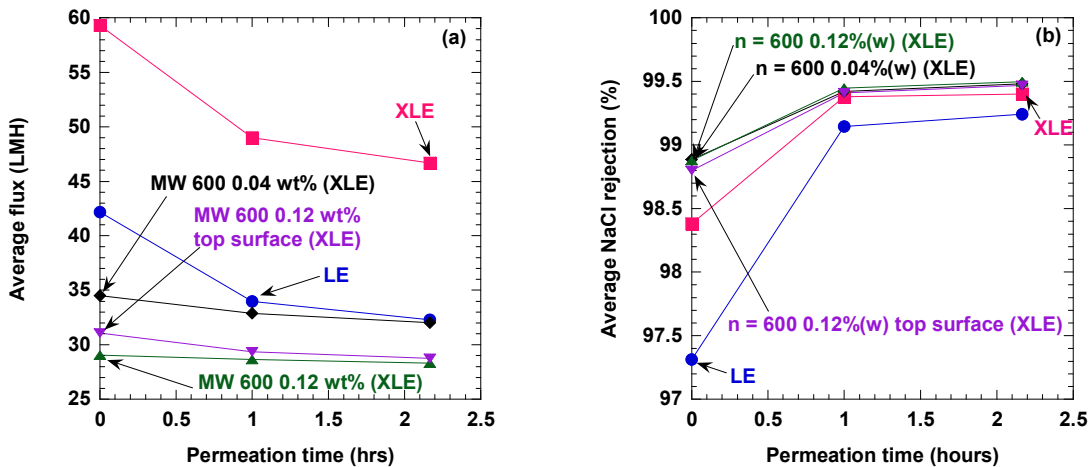
Figure 30. (a) Average flux and **(b)** average NaCl rejection of PEG diepoxide-treated XLE and control LE and XLE membranes in 2000 ppm NaCl plus 25 ppm dodecane/25 ppm SLS emulsion.

Figure 31a shows the water flux versus time for XLE membranes dip treated with 0.04 and 1.0%(w) MW 200 PEG diepoxide. It was thought that using a shorter chain length PEG diepoxide than the experiment shown in Figure 30 would cause the modified XLE membrane to have higher water flux. The test was conducted at 150 psig and a flowrate of 0.85 gpm. The membranes were first tested in pure water feed for approximately 20 hours, then 2000 ppm NaCl was added and flux was monitored for an additional 20 hours. Finally, 20 ppm of DTAB foulant was added to the feed to monitor the fouling resistance of the modified membranes. The feed pH was 7 for both the NaCl and NaCl + DTAB feeds. The flux profile for a control XLE membrane tested previously under the

same conditions is shown in Figure 31 for comparison. While the flux of the modified membranes did not surpass that of the unmodified membrane in the fouling feed, one of the modified membranes did have slightly better fouling resistance than the unmodified membrane. Figure 31b gives the flux of each membrane in the fouling feed normalized to the flux in 2000 ppm NaCl, which eliminates flux differences attributed to the different levels of mass transfer resistance of modified and unmodified membranes. From this perspective it is clear that the 1.0%(w) PEG diepoxide-grafted XLE retains more of its initial flux in the fouling feed than the unmodified XLE. All membranes, modified and unmodified, had observed salt rejections better than 98%.
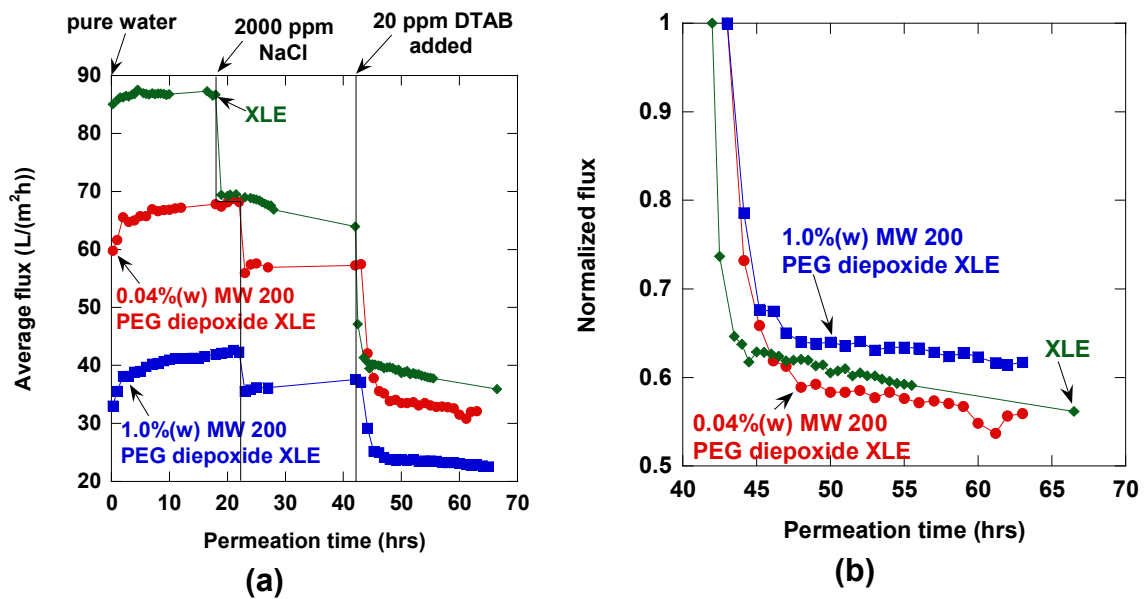
Figure 31. (a) Water flux of MW200 PEG diepoxide-grafted XLEs (dip treatment) and control XLE in pure water, 2000 ppm NaCl, and 2000 ppm NaCl + 20 ppm DTAB feeds (pure water and 2000 ppm NaCl feeds run through carbon/particle prefilter, Δp = 150 psig, feed flowrate = 1.0 gpm, 25°C); **(b)** Fouling resistance of the membranes upon addition of DTAB to the feed (where flux is normalized to average flux in 2000 ppm NaCl).

LE membranes were also used as controls for comparison to PEG diepoxide-grafted XLE membranes. The LE membrane is very similar to the XLE membrane, but with lower flux than the XLE. The extent of fouling a membrane experiences is likely dependent on the amount of water it processes. Therefore, comparing modified XLE membranes, whose flux is lower because of the additional mass transfer resistance provided by the grafted molecules, to LE membranes could eliminate differences in water throughput between the modified and control membranes. The water flux properties of a PEG diepoxide-grafted XLE (dip coated in a 40°C solution of 0.04%(w) MW 200 PEG diepoxide for 10 minutes) and an unmodified LE membrane are compared in Figure 32a. Both membranes have similar water fluxes in pure water and 2000 ppm NaCl

feeds, so the LE is a good choice of control membrane for comparison to the PEG diepoxide-grafted XLE. The membranes' fouling behavior when 20 ppm DTAB is added to the feed is also shown, indicating the modified XLE has higher flux than the control LE. The flux decline experienced by each of the membranes is another means of comparison of their fouling resistance. In Figure 32b, the flux after addition of DTAB is normalized by the average flux observed in 2000 ppm NaCl feed. This method of comparison clearly shows that the PEG diepoxide-grafted XLE retains approximately 5% more of its flux and experiences less fouling than the control LE membrane.
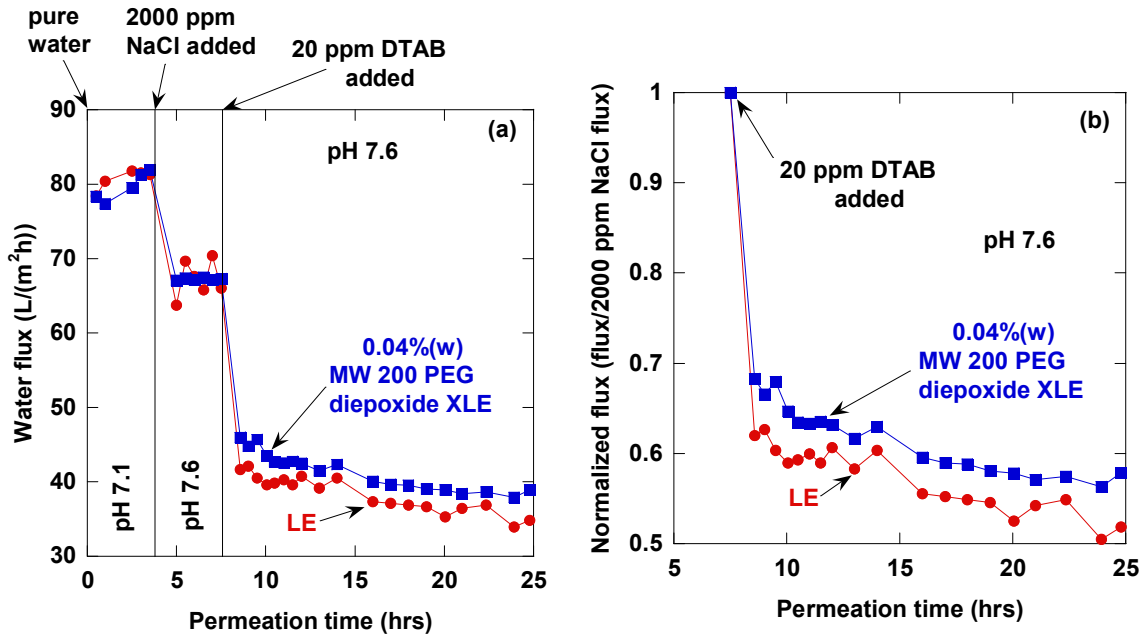

Figure 32. **(a)** Water flux of a MW 200 PEG diepoxide-grafted XLE (dip treatment) and control LE in pure water, 2000 ppm NaCl, and 2000 ppm NaCl + 20 ppm DTAB feeds (pure water and 2000 ppm NaCl feeds run through carbon/particle prefilter, Δp = 150 psig, feed flowrate = 1.0 gpm, 25°C); **(b)** Fouling resistance of the two membranes upon addition of DTAB to the feed (where flux is normalized to average flux in 2000 ppm NaCl).

Table 8 gives the observed NaCl rejection values for the two membranes in the 2000 ppm NaCl and 2000 ppm NaCl + 20 ppm DTAB feeds introduced during the course of the experiment depicted in Figure 32. The control LE and PEG diepoxide-grafted XLE membranes have similar salt rejection properties, indicating grafting has no negative effect on rejection. Additionally, both membranes show a marked increase in NaCl rejection upon addition of DTAB, which is likely caused by DTAB blockage of the membrane surface, preventing NaCl from reaching and diffusing through the membrane. Organic rejection of 100% was measured for both the control LE and PEG diepoxide-grafted XLE membranes.

Table 8. Observed NaCl rejection values of control LE and PEG diepoxide-grafted XLE membranes in 2000 ppm NaCl and 2000 ppm NaCl + 20 ppm DTAB feeds, corresponding to the experiment shown in Figure 32.

	Observed NaCl rejection (%)	
	2000 mg/L NaCl feed	20 ppm DTAB + 2000 mg/L NaCl feed
LE	98.8	99.5
PEG-grafted XLE	98.7	99.3

Crossflow fouling studies of PEG diepoxide-grafted GE AG RO membranes were also conducted to enable comparison of the two surface modification methods, grafting and coating, for the same base membrane. Figure 33a shows the water flux versus time for an unmodified AG membrane (heated to 40°C for better comparison to the modified membranes, which are treated at 40°C) and AG membranes grafted with 0.04 and 10%(w) MW 200 PEG diepoxide. One high (10%(w)) concentration-grafted membrane was tested in this fouling experiment to determine whether extensive surface coverage provides significantly improved fouling resistance which overcomes the negative effect on water flux. The test was conducted at 225 psig (optimum pressure for AG membrane operation) and a flowrate of 1.0 gpm. The membranes were first tested in pure water feed for approximately 4 hours, then 2000 mg/L NaCl was added and flux was monitored for an additional 4 hours. Finally, 20 ppm of DTAB foulant was added to the feed to monitor the fouling resistance of the three membranes. The feed pH was between 7 and 9 for both the NaCl and NaCl + DTAB feeds. Similar to the results of the experiments discussed previously, the flux of the modified AG membranes did not surpass that of the unmodified membrane in the fouling feed, but the modified membranes again had slightly better fouling resistance than the unmodified membrane. Figure 33b gives the flux of each membrane in the fouling feed normalized to the flux in 2000 mg/L NaCl, which clearly shows that both modified membranes had better fouling resistance than the unmodified membrane, with higher concentration PEG diepoxide leading to higher fouling resistance. However, the flux of the 10%(w) PEG diepoxide-grafted AG membrane was too low to be useful, even with its slightly higher fouling resistance.
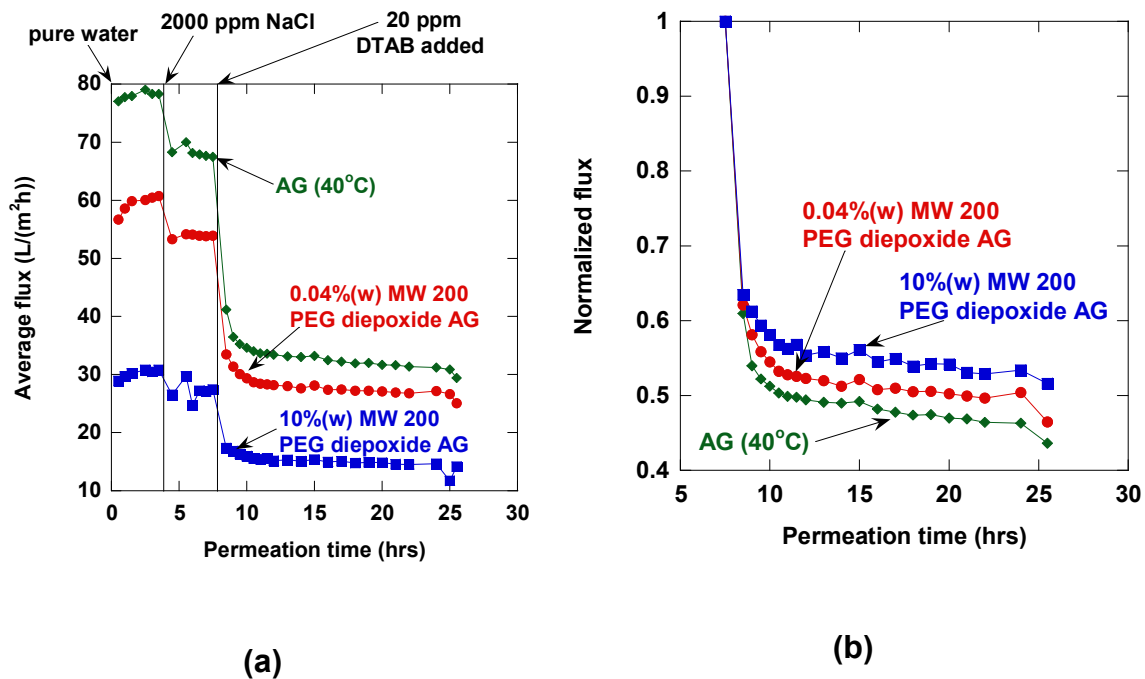
Figure 33. (a) Water flux of MW200 PEG diepoxide-grafted AGs (dip treatment) and control AG in pure water, 2000 ppm NaCl, and 2000 ppm NaCl + 20 ppm DTAB feeds (pure water and 2000 ppm NaCl feeds run through carbon/particle prefilter, Δp = 225 psig, feed flowrate = 1.0 gpm, 25°C); **(b)** Fouling resistance of the two membranes upon addition of DTAB to the feed (where flux is normalized to average flux in 2000 ppm NaCl).

The experimental protocol followed in fouling experiments with top-surface PEG diepoxide-grafted NF90 membranes is given in Figure 34. Pure water flux was first measured for four hours, followed by water flux in 2000 ppm NaCl. The feed was continuously filtered through a carbon and particle filter for the first eight hours of the experiment. Then, when the foulant was introduced (sodium dodecyl sulfate (SDS) or dodecyltrimethylammonium bromide (DTAB)), the filter was bypassed and flux decline was monitored for 16-18 hours. After the fouling portion of the experiment, a cleaning procedure was performed using a fresh pure water feed, once again filtered through the carbon and particle filter. The feed pH was raised using 5%(w) NaOH and after one hour, the feed pH was lowered using 1M HCl. After one hour of operation at low pH, the feed was replaced with a fresh 2000 ppm NaCl feed and water flux and NaCl rejection were measured to determine the recovery of each membrane after cleaning. Temperature was maintained at 24-25°C at all times, with the exception of during the high pH portion of the cleaning procedure. In each experiment, the behavior of two NF90 membranes modified with aqueous solutions of MW 1000 PEG diepoxide was compared to that of a control LE membrane.
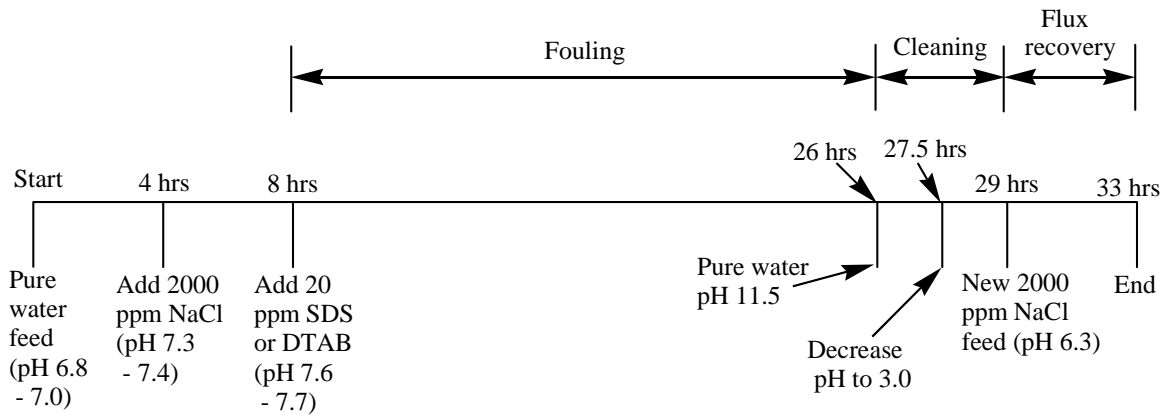
Figure 34. Fouling experiment timeline.

Figure 35 shows the results of fouling experiments using 20 ppm SDS as the foulant. Figures 35(a) and 35(c) give the measured water flux for all portions of the experiment (vertical lines correspond to the experimental protocol given in Figure 34), and Figures 35(b) and 35(d) show the water flux during the fouling and flux recovery portions of the experiment, normalized to the average water flux measured in the initial 2000 ppm NaCl feed (hours 4-8). Although the fluxes of the NF90 membranes grafted with 1% and 5%(w) MW 1000 PEG diepoxide are clearly higher than the control LE during the fouling portion of the experiment (Figure 35(a)), the fouling resistance of the NF90 membranes grafted with 10% and 15%(w) MW 1000 PEG diepoxide relative to the control LE is not as obvious (Figure 35(c)). Figures 35(b) and 35(d) more clearly demonstrate the higher fouling resistance of all four modified NF90 membranes. Additionally, these figures show that while the LE membrane experiences irreversible fouling (as evidenced by only 85% flux recovery after cleaning), the modified NF90 membranes have no irreversible fouling. The NaCl and organic rejections of all membranes (control LE and modified NF90) were similar to each other and greater than 98%, so MW 1000 PEG diepoxide was again demonstrated capable of increasing the rejection of the NF90 membrane to a level comparable to that of the LE membrane.
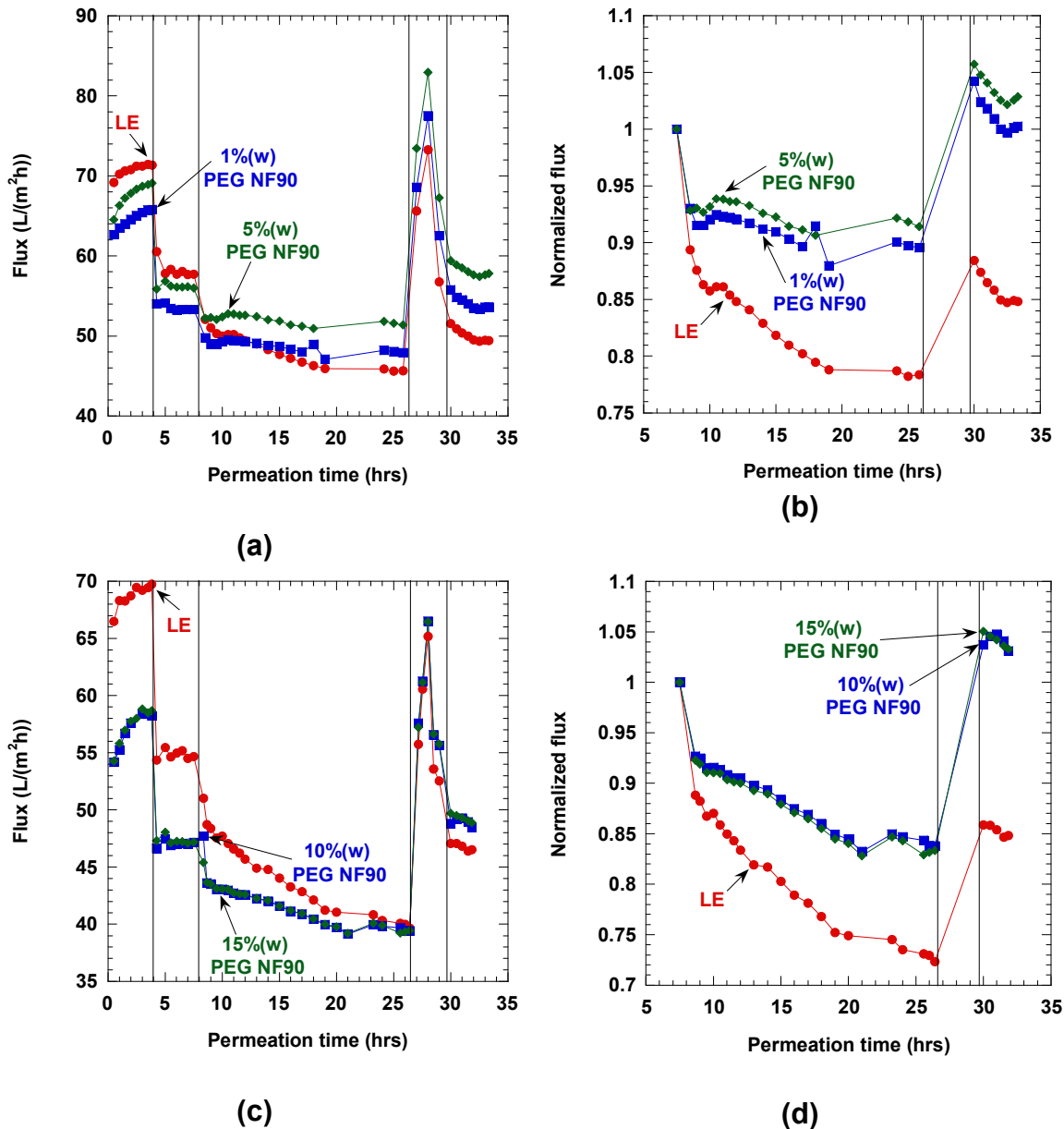
Figure 35. SDS fouling resistance of NF90 membranes top surface-treated with MW 1000 PEG diepoxide compared to control LE membranes. **(a)** and **(c)** Water flux; **(b)** and **(d)** Water flux normalized to average water flux in initial 2000 ppm NaCl feed (Δp = 150 psi, flowrate = 1.0 gpm).

Figure 36 shows the results of fouling experiments using 20 ppm DTAB as the foulant. Figures 36(a) and 36(c) give the measured water flux for all portions of the experiment (vertical lines correspond to the experimental protocol given in Figure 34), and Figures 36(b) and 36(d) show the water flux during the fouling and flux recovery portions of the experiment, normalized to the average water flux measured in the initial 2000 ppm NaCl feed (hours 4-8). Comparison of Figures 35 and 36 demonstrates that DTAB fouls more severely than SDS. However, as in the SDS fouling experiments, the modified NF90 membranes showed better fouling resistance (less flux decline) and better flux recovery (no irreversible fouling) than the control LE membrane.
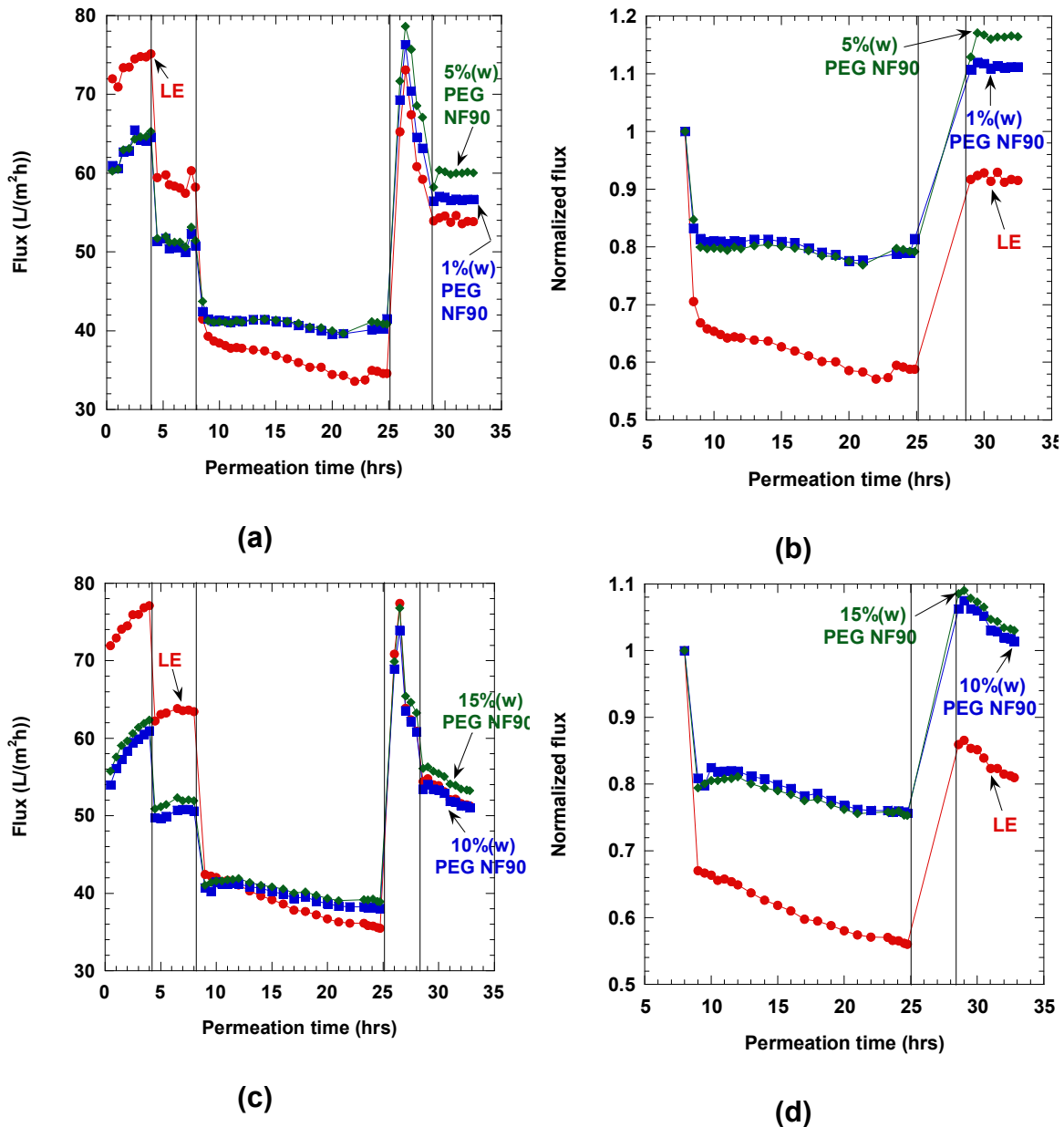
41

Figure 36. DTAB fouling resistance of NF90 membranes top surface-treated with MW 1000 PEG diepoxide compared to control LE membranes. **(a)** and **(c)** Water flux; **(b)** and **(d)** Water flux normalized to average water flux in initial 2000 ppm NaCl feed (Δp = 150 psi, flowrate = 1.0 gpm).

Figures 35(b), 35(d), 36(b), and 36(d) indicate that the modified NF90 membranes not only have no irreversible fouling, their water fluxes are actually higher after cleaning than they were initially (normalized flux is greater than 1). In addition, the final NaCl rejections of the modified NF90 membranes were 0.5-1.0% lower than the initial values. These two observations were hypothesized to be due to removal of residual adsorbed PEG diepoxide (i.e., PEG diepoxide that did not react with the membrane surface). In order to determine whether more PEG diepoxide would be removed from the surface with multiple fouling/cleaning procedures (as would be used in actual practice), an experiment with two

42

fouling/cleaning cycles was performed. The procedure outlined in Figure 34 was followed, simply repeating the fouling/cleaning/flux recovery portion of the experiment twice. As seen in Figure 37, the modified NF90 membranes' fluxes did not increase any further after the second cycle. Also, their NaCl rejections did not decrease any further, so it appears that while some adsorbed PEG is removed during the initial use of the modified membranes, the grafted PEG remains attached to the membrane surface and can be expected to withstand multiple fouling/cleaning cycles.
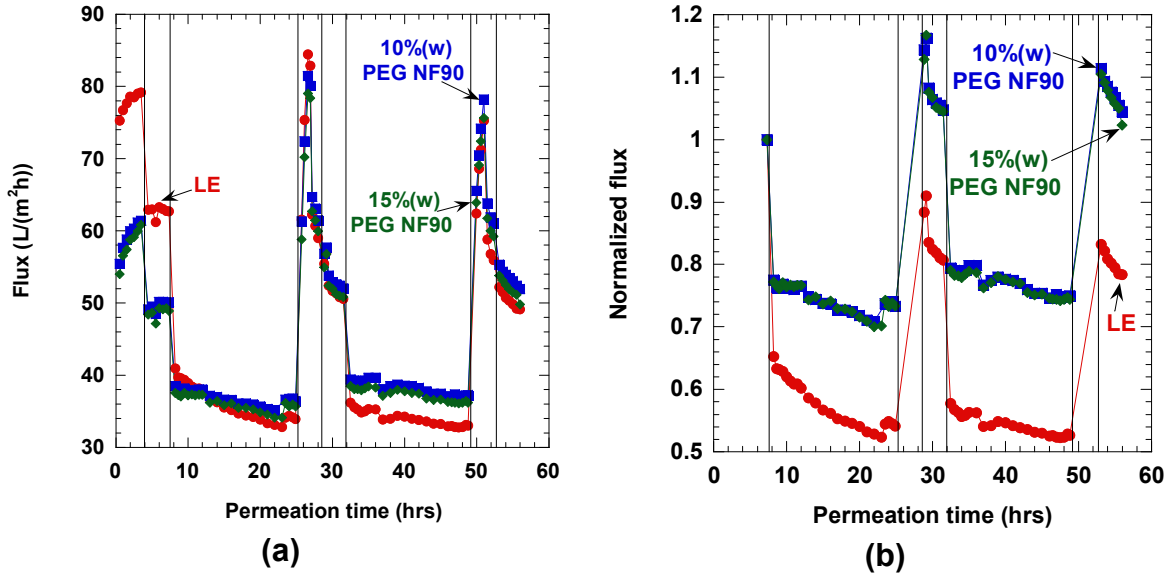
(a)   **(b)**

Figure 37. DTAB fouling resistance of NF90 membranes top surface-treated with MW 1000 PEG diepoxide, where the fouling/cleaning/flux recovery cycle has been performed twice. **(a)** Water flux and **(b)** Water flux normalized to average water flux in initial 2000 ppm NaCl feed (Δp = 150 psi, flowrate = 1.0 gpm).

Finally, results from a series of experiments comparing the fouling resistance of control LE and modified NF90 membranes in fouling solutions of increasing DTAB concentration are given in Figure 38. The NF90 membranes were top surface-treated with 1 and 15%(w) aqueous solutions of MW 1000 PEG diepoxide. Figure 38a presents the fouling resistance, or flux retention, as a function of DTAB concentration, while Figure 38b presents the flux recovery as a function of DTAB concentration. Figure 38a demonstrates that the modified NF90 membranes showed consistently higher fouling resistance (10-20% higher flux retention) than control LE membranes at DTAB concentrations up to 250 ppm. Also, Figure 38b shows that the control LE membrane experiences worsening irreversible fouling with increasing DTAB concentration, while the modified NF90 membranes show no irreversible fouling at DTAB concentrations up to 250 ppm. Therefore, the modified NF90 membranes outperform the control LE membranes in terms of fouling resistance and the ability to clean off the foulants that do adhere to the membrane during the fouling test. Surface grafting with PEG diepoxide appears to be a feasible means of improving the fouling performance of commercial membranes.
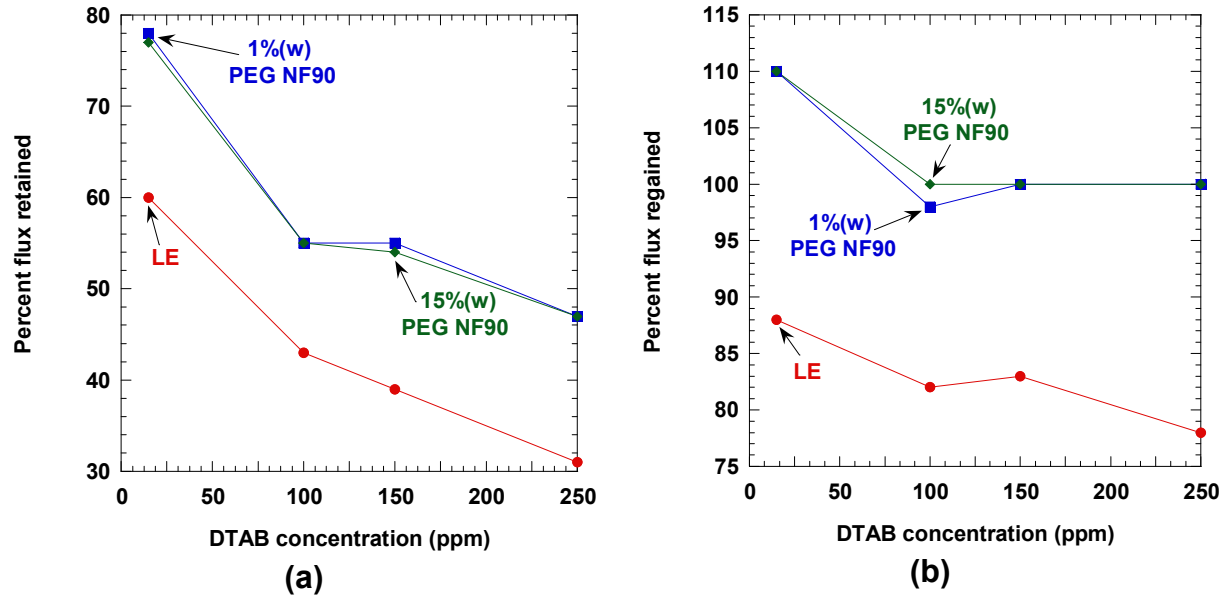
Figure 38. DTAB fouling resistance of NF90 membranes top surface-treated with MW 1000 PEG diepoxide compared to control LE membranes, for experiments using different concentrations of DTAB fouling feed solution. **(a)** Fouling resistance, or flux retention during fouling, as a function of DTAB feed concentration and **(b)** Flux recovery after cleaning fouled membranes as a function of DTAB feed concentration (Δp = 150 psi, flowrate = 1.0 gpm).

CONCLUSION

This work provides answers to some of the fundamental questions posed regarding the viability of using modified membranes for produced water treatment. The project goals were met and significant progress was made towards implementing membranes in produced water treatment. Systematic studies were done on potential coating materials to explore the relationships between chemical structure and material properties, and ultimately how the structure relates to fouling resistance. Through these studies, ways to tailor materials to reach a desired set of properties were developed. Surface grafting was attempted as a less-problematic alternative to coating, and a better understanding of important variables was gained. Characterization of unmodified and surface-modified membranes unveiled a need to solidify basic RO membrane testing and reporting procedures. While this work was tedious and did not lend itself directly to produced water treatment, the careful attention to detail and thorough understanding of important experimental factors will significantly increase the credibility of all future data.   Overall, the data amassed in the project term should serve as a substantial resource to support future research on membranes and produced water treatment.

GRAPHICAL MATERIALS

Tables

Figures

Figure 32. **(a)** Water flux of a MW 200 PEG diepoxide-grafted XLE (dip treatment) and control LE in pure water, 2000 ppm NaCl, and 2000 ppm NaCl + 20 ppm DTAB feeds (pure water and 2000 ppm NaCl feeds run through carbon/particle prefilter, Δp = 150 psig, feed flowrate = 1.0 gpm, 25°C); **(b)** Fouling resistance of the two membranes upon addition of DTAB to the feed (where flux is normalized to average flux in 2000 ppm NaCl).

Figure 33. **(a)** Water flux of MW200 PEG diepoxide-grafted AGs (dip treatment) and control AG in pure water, 2000 ppm NaCl, and 2000 ppm NaCl + 20 ppm DTAB feeds (pure water and 2000 ppm NaCl feeds run through carbon/particle prefilter, Δp = 225 psig, feed flowrate = 1.0 gpm, 25°C); **(b)** Fouling resistance of the two membranes upon addition of DTAB to the feed (where flux is normalized to average flux in 2000 ppm NaCl).

Figure 34. Fouling experiment timeline.

Figure 35. SDS fouling resistance of NF90 membranes top surface-treated with MW 1000 PEG diepoxide compared to control LE membranes. **(a)** and **(c)** Water flux; **(b)** and **(d)** Water flux normalized to average water flux in initial 2000 ppm NaCl feed (Δp = 150 psi, flowrate = 1.0 gpm).

Figure 36. DTAB fouling resistance of NF90 membranes top surface-treated with MW 1000 PEG diepoxide compared to control LE membranes. **(a)** and **(c)** Water flux; **(b)** and **(d)** Water flux normalized to average water flux in initial 2000 ppm NaCl feed (Δp = 150 psi, flowrate = 1.0 gpm).

Figure 37. DTAB fouling resistance of NF90 membranes top surface-treated with MW 1000 PEG diepoxide, where the fouling/cleaning/flux recovery cycle has been performed twice. **(a)** Water flux and **(b)** Water flux normalized to average water flux in initial 2000 ppm NaCl feed (Δp = 150 psi, flowrate = 1.0 gpm).

Figure 38. DTAB fouling resistance of NF90 membranes top surface-treated with MW 1000 PEG diepoxide compared to control LE membranes, for experiments using different concentrations of DTAB fouling feed solution. **(a)** Fouling resistance, or flux retention during fouling, as a function of DTAB feed concentration and **(b)** Flux recovery after cleaning fouled membranes as a function of DTAB feed concentration (Δp = 150 psi, flowrate = 1.0 gpm).

REFERENCES

[1]   Product Information: GE Osmonics AG Desal Membranes,
        http://www.desal.com, (2004).

[2]   Dow FILMTEC BW30LE-440 Product Specification,
        http://www.dow.com/liquidseps/prod/bw30le_440.htm, (2007).

[3]   Dow FILMTEC XLE-440 Product Specification,
        http://www.dow.com/liquidseps/prod/xle_440.htm, (2007).

[4]   H. Lin, E. Van Wagner, J. S. Swinnea, B. D. Freeman, S. J. Pas, A. J.
        Hill, S. Kalakkunnath and D. S. Kalika, Transport and structural
        characteristics of crosslinked poly(ethylene oxide) rubbers, Journal
        of Membrane Science 276 (2006) 145-161.

[5]   Optics and optical instruments: contact lenses-determination of
        thickness Part II: Hydrogel contact lenses, ISO 9339-2, (1998).

[6]   K. Nagai, et al., Solubility and diffusivity of sodium chloride in phase-
        separated block copolymers of poly(2-dimethylaminoethyl
        methacrylate), poly(1,1'-dihydroperfluorooctyl methacrylate), and
        poly(1,1,2,2-tetrahydroperfluorooctyl acrylate), Polymer 42 (2001)
        9941-9948.

[7]   H. Yasuda, C. E. Lamaze and L. D. Ikenberry, Permeability of solutes
        through hydrated polymer membranes. Part I: Diffusion of sodium
        chloride, Die Makromolekulare Chemie 118 (1968) 19-35.

[8]   R. B. Bird, W. E. Stewart and E. N. Lightfoot, Transport Phenomena,
        2nd ed., John Wiley & Sons, Inc., New York, (2002).

[9]   J. Crank and G. S. Park, Methods of Measurement, in J. Crank and G. S. Park (Eds.), Diffusion in Polymers, Academic Press, Inc., New York, (1968).

[10]   W. E. Mickols, Composite Membrane with Polyalkylene Oxide Modified Polyamide Surface., US Patent US 6,280,853 B1, (2001).

[11]   R. W. Baker, Membrane Technology and Applications, 2nd ed., John Wiley & Sons, Ltd., Chichester, (2004).

[12]   I. Sutzkover, D. Hasson and R. Semiat, Simple technique for measuring the concentration polarization level in a reverse osmosis system, Desalination 131 (2000) 117-127.

[13]   S. K. Bajpai and S. Singh, Analysis of swelling behavior of poly(methacrylamide-co-methacrylic acid) hydrogels and effect of synthesis conditions on water uptake, React. Funct. Polym. 66 (2006) 431-440.

[14]   N. B. Graham, Poly(ethylene oxide) and related materials, in N. A. Peppas (Ed.), Hydrogels in Medicine and Pharmacy, Vol. II: Polymers, CRC Press, Boca Raton, (1987), pp. 95-113.

[15]   H. S. Ashbaugh and M. E. Paulaitis, Monomer hydrophobicity as a mechanism for the LCST behavior of poly(ethylene oxide) in water, Ind. Eng. Chem. Res. 45 (2006) 5531-5537.

[16]   J. B. Thomas, J. H. Tingsanchali, A. M. Rosales, C. M. Creecy, J. W. McGinty and N. A. Peppas, Dynamics of poly(ethylene glycol)-tethered, pH responsive networks, Polymer 48 (2007) 5042-5048.

[17]   O. Okay, Macroporous copolymer networks, Progress in Polymer Science 25 (2000) 711-779.

[18]   C. J. D. Fell and H. P. Hutchinson, Diffusion coefficients for sodium and potassium chlorides in water at elevated temperatures, Journal of Chemical and Engineering Data 16 (1971) 427-429.

[19]   A. W. Adamson and A. P. Gast, Physical Chemistry of Surfaces, 6th ed., John Wiley & Sons, Inc., New York, (1997).

[20]   H. Ju, B. D. McCloskey, A. C. Sagle, Y. H. Wu, V. Kusuma and B. D. Freeman, Crosslinked poly(ethylene oxide) fouling resistant coating materials for oil/water separation, Journal of Membrane Science In Press (2007).

ACRONYMS AND ABBREVIATIONS

AA	acrylic acid
AFM	atomic force microscopy
DCF193	Dow Corning Fluid 193
DTAB	dodecyltrimethylammonium bromide
EO	ethylene oxide
FTIR	Fourier transform infrared spectroscopy
HEA	2-hydroxyethylacrylate
HPK	1-hydroxycyclohexylphenylketone
NF	nanofiltration
PDI	polydispersity index
PEG	poly(ethylene glycol)
PEG diepoxide	poly(ethylene glycol) diglycidyl ether
PEGA	poly(ethylene glycol) acrylate
PEGDA	poly(ethylene glycol) diacrylate
PEO	poly(ethylene oxide) –same as PEG, means multiple EO units
RO	reverse osmosis
SDS	sodium dodecylsulfate
SEM	scanning electron microscopy
TOC	total organic carbon
UF	ultrafiltration
XPS	x-ray photoelectron spectroscopy

APPENDIX: Report of produced water analysis

Sample NG-1 is natural gas well
Sample OW-1 is oil well

<u>REPORT OF ANALYSIS</u>

DISSOLVED METALS

LAB NUMBER	K0275	K0276			
SAMPLE ID	NG-1 6-1-05 11:00AM	OW-1 6-1-05 10:00AM	Reporting Limit, mg/L	Method	Date Analyzed
Aluminum, mg/L	3.3	0.75	1.0	6010C	6/9/2005
Barium, mg/L	ND	ND	1.0	6010C	6/8/2005
Beryllium, mg/L	0.09	< 0.05	0.05	6010C	6/9/2005
Boron, mg/L	7	17	1.0	6010C	6/9/2005
Bromide, mg/L	ND	ND	50	6010C	6/22/2005
Cadmium, mg/L	0.5 J	ND	1.0	6010C	6/8/2005
Calcium, mg/L	660	4780	1.0	6010C	6/6/2005
Chromium, mg/L	2.4	1.7	1.0	6010C	6/8/2005
Cobalt, mg/L	ND	ND	1.0	6010C	6/9/2005
Copper, mg/L	ND	ND	1.0	6010C	6/9/2005
Iron, mg/L	23	2.5	1.0	6010C	6/6/2005
Magnesium, mg/L	194	1117	1.0	6010C	6/6/2005
Manganese, mg/L	4.2	1.2	1.0	6010C	6/9/2005
Nickel, mg/L	2.7	0.5 J	1.0	6010C	6/9/2005
Potassium, mg/L	77	855	1.0	6010C	6/6/2005
Silicon, mg/L	15.2	6.06	1.0	6010C	6/6/2005
Sodium, mg/L	4,272	61,440	1.0	6010C	6/6/2005
Strontium, mg/L	27.2	85.7	1.0	6010C	6/9/2005
Vanadium, mg/L	2	3	1.0	6010C	6/9/2005
Zinc, mg/L	2.8	1.8	1.0	6010C	6/9/2005
Lithium, mg/L	2.5	15.3	1.0	6010C	6/9/2005
Uranium, mg/L	ND	ND	5.0	6010C	6/9/2005
Silver, mg/L	ND	ND	1.0	6010C	6/8/2005
Arsenic, mg/L	ND	ND	1.0	6010C	6/8/2005
Mercury, mg/L	ND	ND	0.05	6010C	6/8/2005
Lead, mg/L	1.2	0.5 J	1.0	6010C	6/8/2005
Selenium, mg/L	ND	ND	1.0	6010C	6/8/2005

J: Estimated value; detected below reporting limit.

REPORT OF ANALYSIS

LAB NUMBER	K0275	K0276			
SAMPLE ID	NG-1 6-1-05	OW-1 6-1-05	Reporting	Method	Date
Ammonia, mg/L	8	23	5	350.3	6/14/2005
Chloride, mg/L	7,880	153,000	10	300.0	6/6/2005
Fluoride, mg/L	64	133	10	300.0	6/6/2005
Nitrate as N, mg/L	59	ND	10	300.0	6/6/2005
Nitrite as N, mg/L	142	ND	10	300.0	6/6/2005
Phosphate as P, mg/L	144	ND	10	300.0	6/6/2005
Sulfate, mg/L	874	2,580	10	300.0	6/6/2005
pH, su	8	7	NA	310.1	6/6/2005
Carbonate (as $CaCO_3$), mg/L	0	0	NA	310.1	6/6/2005
Bicarbonate (as $CaCO_3$), mg/L	827	320	NA	310.1	6/6/2005
Total Alkalinity (as $CaCO_3$), mg/L	827	320	NA	310.1	6/6/2005
Total Dissolved Solids, mg/L	15,700	227,000	10	160.1	6/7/2005
Total Suspended Solids, mg/L	62	40	10	160.1	6/8/2005
Conductivity, umhos/cm	27,100	392,000	5	120.1	6/7/2005
TRPH, mg/L	20	21	2.0	1664	6/7/2005
Phenols, mg/L	ND	ND	0.5	420.1	6/3/2005
Hydrogen Sulfide, mg/L	140	135	0.5	9215	6/14/2005
Total Organic Carbon, mg/L	1,650	106	5	415.1	6/6/2005
Heterotropic Bacteria MPN/100ml	470,000	116,000	NA	9215B	6/4/2005